NIST-GCR-93-624

An Experimental Study of Multiple Droplet Evaporative Cooling

H. Dawson
M. di Marzo

Grant 70NANB1H1173

NIST

NIST-GCR-93-624

An Experimental Study of Multiple Droplet Evaporative Cooling

H. Dawson
M. di Marzo

University of Maryland
Mechanical Engineering Department
College Park, MD 20742

Final Report
December 1992

Issued April 1993

Sponsored by:
U.S. DEPARTMENT OF COMMERCE
Technology Administration
National Institute of Standards
and Technology
Building and Fire Research Laboratory
Gaithersburg, MD 20899

U.S. DEPARTMENT OF COMMERCE
Ronald H. Brown, Secretary

NATIONAL INSTITUTE OF STANDARDS AND TECHNOLOGY
Raymond G. Kammer, Acting Director

Notice

This report was prepared for the Building and Fire Research Laboratory of the National Institute of Standards and Technology under grant number 70NANB1H1173. The statements and conclusions contained in this report are those of the authors and do not necessarily reflect the views of the National Institute of Standards and Technology or the Building and Fire Research Laboratory.

AN EXPERIMENTAL STUDY OF MULTIPLE DROPLET EVAPORATIVE COOLING

Final Report

H. Dawson, M. di Marzo

Prepared for the

Building and Fire Research Laboratory

National Institute of Standards and Technology

Gaithersburg, MD 20899

Mechanical Engineering Department

Report No. 92-1

University of Maryland

College Park, MD 20742

December 1992

ABSTRACT

Techniques of infrared thermography were used to conduct an experimental study of the evaporative cooling of a hot, low thermal conductivity, non-metallic surface heated by radiation and subject to a random array of impinging water droplets. A droplet generating and distributing apparatus and a data acquisition system employing digital image analysis devices were also developed and implemented. Real time infrared images of the heated surface were recorded and digitized using computer resident frame grabbing hardware and analyzed on a pixel by pixel basis, giving a high degree of thermal and spatial resolution. From these analyses, the instantaneous surface temperature distribution and transient surface temperature profile were obtained for a range of initial temperatures and impinging mass fluxes. The surface temperature was found to decay exponentially with time to a steady state value for the fluxes used. Three dimensional plots of the temperature distribution on the surface also showed the significant lowering of the average surface temperature, and provided a qualitative description of the cooling phenomena at various stages during the transient. Results obtained will be used in the future validation of a computer model of the phenomena.

FOREWORD

This report describes the research performed during the period September 1991 - December 1992 under a joint research program between the Mechanical Engineering Department of the University of Maryland and the Center for Fire Research of the National Institute of Standards and Technology. The research was conducted in the laboratories of the BFRL by Mr. Howard Dawson, a Graduate Research Assistant of the ME Department, under the joint supervision of Dr. Marino di Marzo (ME Dept. - UMCP) and Dr. David D. Evans (BFRL - NIST). This report also constitutes the Master Thesis of Mr. Dawson, which has been completed and defended in the month of November 1992.

LIST OF TABLES

LIST OF FIGURES

1. INTRODUCTION AND PURPOSE

There are a number of engineering applications in which a hot surface is subject to a spray of water droplets. Due to the latent heat needed to vaporize the water, evaporation of the droplets allows very large amounts of heat to be removed from the surface. Cooling by such means is typically referred to in the literature as spray cooling, multiple droplet evaporative cooling, or simply evaporative cooling.

Evaporative cooling is utilized in a variety of industrial and scientific applications. In the field of metallurgy, it is used in the quenching of hot metals. The nuclear power industry employs it in liquid metal heat transfer systems. More recent use has been found by the National Aeronautics and Space Administration in the environmental control system of the Space Shuttle. Grissom and Weirum provide an investigation of spray cooling for this purpose in reference [1].

Another application for which the study of spray cooling is relevant is in steam generator boiler tubes. Levitan and Lantsman conduct a study of steam flow in a pipe in reference [2]. Similar studies involving mist flows may be found in references [3] and [4]. Additionally, the cooling of turbine blades provides a use for spray cooling, as investigated by Savic and Boult in [5].

Previous studies on the more fundamental aspects of droplet evaporation and cooling were conducted by Klassen and diMarzo [6], who looked at the evaporation of a single droplet from a low thermal conductivity surface, with heat input by conduction through surface. Kidder and others [7], [8] extended the single droplet study to the case of radiant heat input from above the droplet. Additional work may be found by Abu-Zaid and Atreya [9], who studied the transient cooling of a low conductivity surface, and by Seki et. al. [10], who investigated the transient temperature profile of hot surface subject to droplet impingement. Bonacina [11] and Makino and Michiyoshi [12] have also done interesting work in the field.

An important application of evaporative cooling is in the field of fire suppression to study the cooling and extinguishment effects of fire sprinklers. It was this application which provided the impetus for the present work. The study was conducted in the laboratories of The National Institute of Standards and Technology in Gaithersburg, Maryland (NIST), and formed part of a joint research effort between the University of Maryland and the Center for Fire Research at NIST.

The purpose of this experimental study was to quantify the transient evaporative cooling of a radiantly heated, low thermal conductivity material subject to a random impingement of water droplets. Specifically, the transient behavior and spatial distribution of

the surface temperature were investigated over a range of initial surface temperatures and impinging mass fluxes. Additionally, it was desired to draw some conclusions about the important parameters in the evaporative cooling phenomenon, and about evaporative cooling generally.

A concurrent goal of the research was to continue development of the infrared thermography and digital image analysis techniques and equipment employed in the data acquisition system. These methods were successfully implemented by Klassen [6], and extended by Kidder [7].

Results obtained here will find future use in the validation of a computer code which forms the other aspect of the project [13]. Presently, the code is valid over a range of conditions for the case of both single and multiple droplets heated from below by conduction. Refinements are currently being made to include the effects of radiation heat input from above the surface.

Important to note is that all experiments conducted here represent a simplified model with respect to spray cooling in a true fire environment. This is necessary to ensure controllable conditions in which to study the phenomenon.

2. EXPERIMENTAL EQUIPMENT AND SETUP

2.1 General Description

The general experimental setup is pictured in Figure 1. A droplet generating device is located above the heated surface such that droplets ejected impact with the surface. The droplet generator works in conjunction with both a positioning mechanism and a water feed system, as labeled in the figure. Radiant panels are mounted around the macor tile to provide the required heat input, and an infrared camera is aimed at the surface for data acquisition. These components will be described in more detail briefly.

While the experimental setup consists of a number of various devices which are necessary for a controlled experiment, there are four primary objectives which need to be met. A major challenge was designing or obtaining equipment to satisfy these objectives. Briefly summarized, they are:

1. Must be able to generate water droplets of repeatable size.
2. Must be able to randomly distribute water droplets on the heated surface.
3. Must have a controllable source of radiant heat to simulate that encountered in a fire environment.
4. Must be able to degas the water and dispense it without introducing new non-condensible gases.

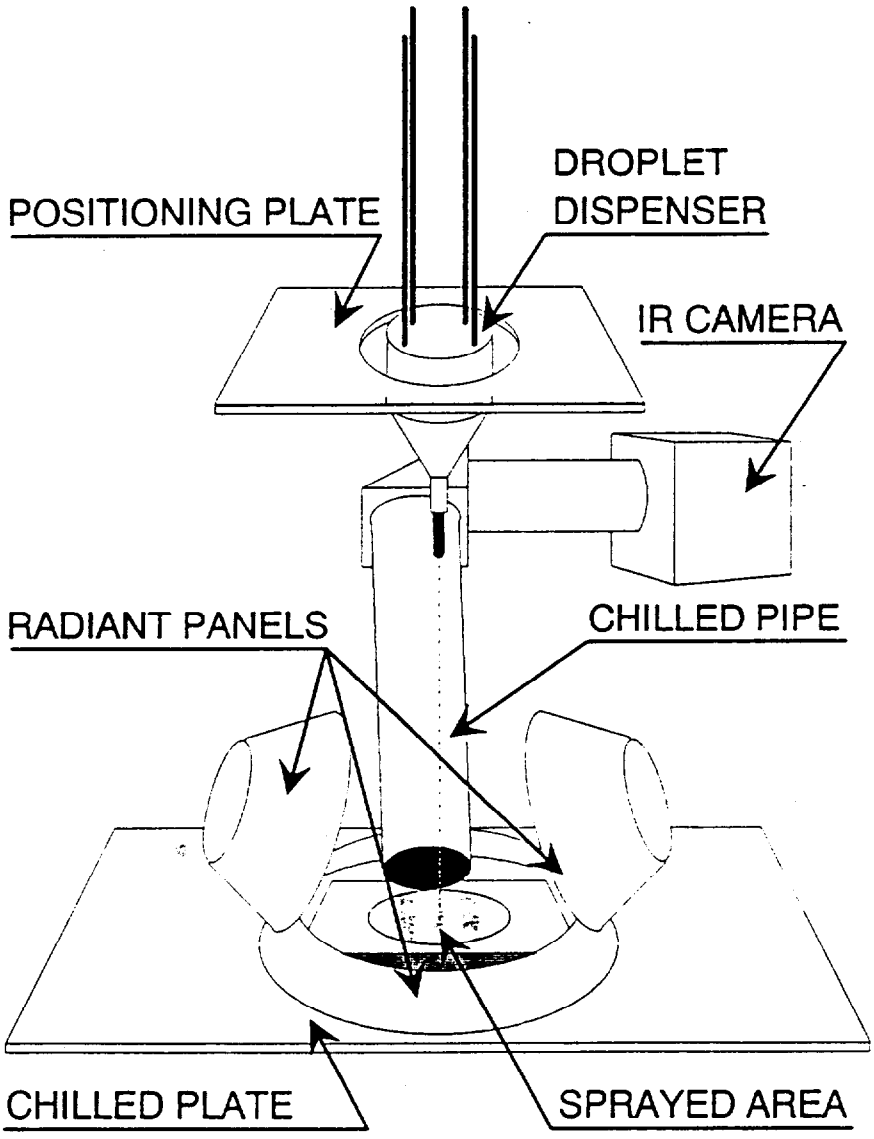

Figure 1 - Experimental Setup

The various apparatus used to achieve the above requirements each warrant individual, detailed description. They will now be discussed in the order above, followed by descriptions of the remaining experimental setup and of the other components used.

2.2 Droplet Generator

The generation of water droplets of controllable and uniform size is perhaps the most important consideration in the experiment. Repeatability in droplet size is essential to ensure an accurate measure of the impinging mass flux to the surface. To this end, a water droplet generator meeting the above criteria was developed. The device was designed and validated by a group of student researchers also working under the author's research advisor [14].

The design of the droplet generator may be seen in Figure 2. The main body of the generator is constructed of aluminum, machined into a cylindrical shape .127 m in diameter and with a gradual taper as shown. A square aluminum top plate is attached to the body with four cap screws, and a .0254 m space is maintained between the bottom of the plate and the top of the body with four copper pipe spacers. There is an internal conical cavity bored through the main body (shown by dashed lines in Figure 2) which exits through a hole on the bottom of the main body. An aluminum core fits above the top of the conical

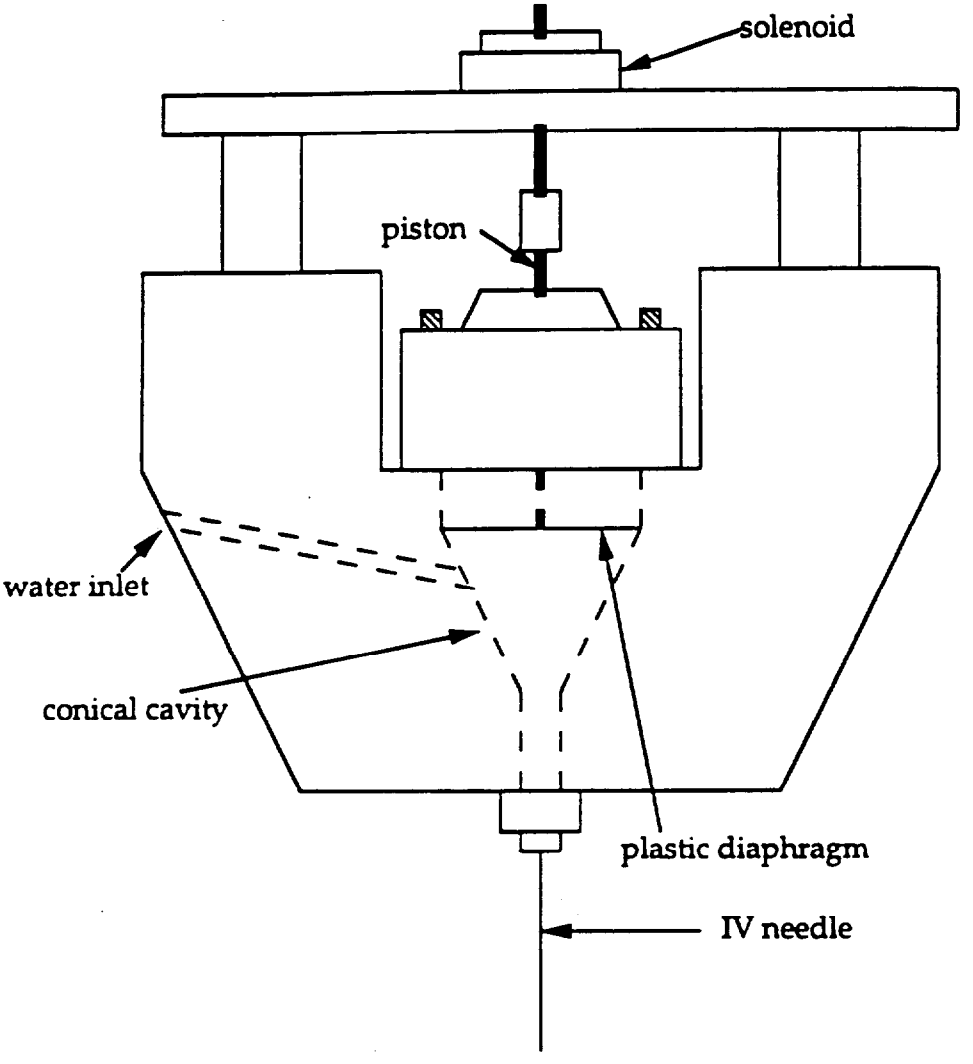

Figure 2 - Droplet Generator

space and is attached with four cap screws. A size 20 IV needle, shortened in its length, is attached at the base of the body with a Swagelock fitting. Water enters the generator through a check valve, consisting of a small plastic ball and spring, which prevents it from flowing back into the feed lines.

The primary mechanism for droplet generation is the conical cavity. The cavity is filled with water, and a plastic diaphragm rests on top of a small ledge at the top of the void, sealing-in the water below. A proper seal is maintained by placing a rubber o-ring on top of the diaphragm and then tightening the aluminum core on top of the o-ring. A hardened steel piston, .0032 m in diameter, is guided by a hole drilled in the core and rests on top of the diaphragm. The top of the piston fits into a spacer consisting of an aluminum cylinder with a small screw on top. The top of the spacer is in turn connected to a solenoid attached to the top plate, and provides a small gap (less than .001 m) between the solenoid core and solenoid body. When energized, the solenoid pushes down on the spacer and closes the gap, thus causing a deflection in the diaphragm and producing a droplet. Precise adjustment of the gap is possible by turning in or out the screw in the spacer.

In order to maintain the most consistent droplet size, it is necessary that the static head of the reservoir feeding water to the generator be set to zero. It was originally thought that droplets could

be formed at smaller volumes if a static head greater than zero were used and the droplets were allowed to grow at the tip of the needle. Before they reached the critical mass at which they would fall on their own, the solenoid would eject them. However, experiments revealed that repeatable sizes could only be achieved with zero static head [14], determined by the point at which water just ceases to drip from the needle tip. That is, the generator must act as a pump.

Droplet size is additionally governed by the bore of the needle, the voltage applied across the solenoid, and the travel of the solenoid. In the experiments conducted, the voltage and needle bore were held constant, leaving the solenoid gap and static head as the adjustable parameters. Power to the solenoid is supplied by a Powermate BP-18F DC voltage supply, and the voltage across the solenoid is held at 8 volts. Voltages higher than this cause the diaphragm to crack. An electronic relay placed between the solenoid and power supply allows control over the frequency at which the solenoid is activated. By adjusting this, the mass flux of the water spray to the surface can be regulated. There is a practical upper limit of 1 Hz for the droplet generation frequency. Although the relay is capable of higher frequencies, ejection of the droplets from the generator becomes erratic at values higher than 1 Hz.

2.3 Random Positioning Plate

In order to more realistically simulate the spray cooling process, it was determined that the distribution of water droplets on the surface should be random over a circular area.

To achieve this distribution, a positioning mechanism for the droplet generator was conceived and built. The idea of operation of the positioning mechanism is to have the droplet generator be vertically suspended by wires and collide with mechanical energizing bumpers within a fixed perimeter. When the generator impacts with one of the bumpers, it swings away and collides with another, and the process continues for sustained motion. With appropriate bumper shape, movement, and impact, the motion of the droplet generator as it swung within the predetermined area can be closely approximated as random over the time scales of the experimental runs.

The final design encompassing the above considerations is a positioning plate with electrically activated bumpers, as shown in Figure 3. The base plate of the positioner was constructed of a (.43 m x .43 m x .0127 m) aluminum sheet with a circular hole .279 m in diameter cut in the center of the plate to provide the space for dropper motion. Three bumpers made of polyethylene sit directly on top of the base plate and are spaced at equal angles around the hole. Guide studs are attached to

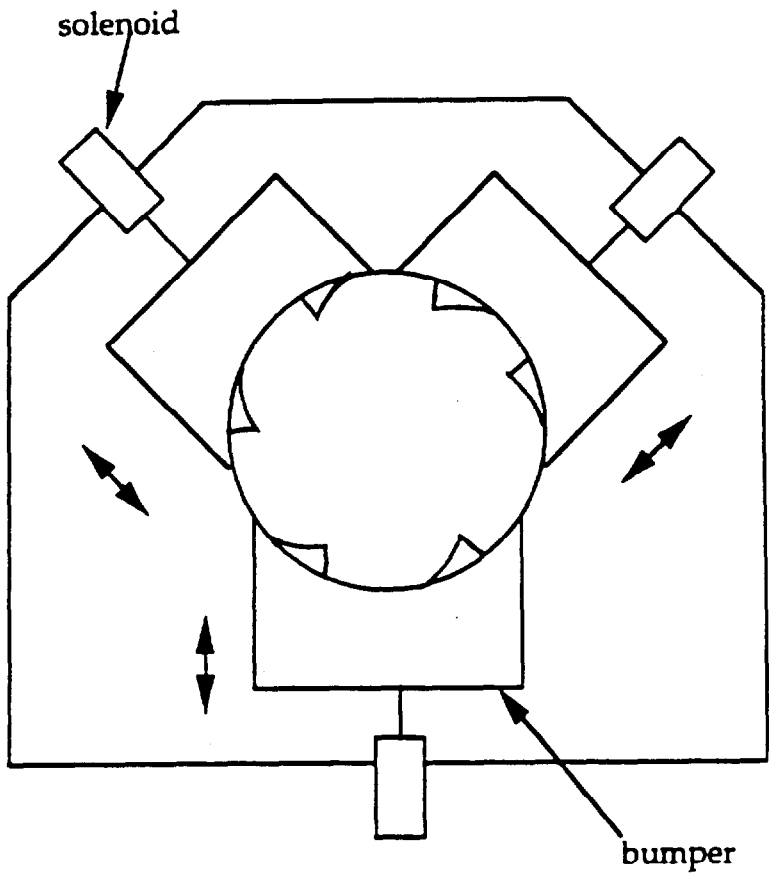

Figure 3 - Positioning Plate

the base plate on each of the bumpers to keep the bumpers traveling in a straight line.

In order to provide bumper motion, solenoids are used. A solenoid is located behind each bumper and attached to the base plate with a mounting bracket, and each bumper attached to its respective solenoid piston. Springs stretched between each bumper and solenoid serve as a return mechanism for the bumpers, retracting them after they move inward to impact with the droplet generator. The travel of each solenoid, and hence bumper, is controlled by an adjusting screw located in the mounting bracket behind the solenoids. Turning this screw adjusts the amount that the solenoid piston protrudes out of the solenoid body, thereby determining the travel when energized. Solenoid travel used in this study is .007 m.

The droplet generator is vertically suspended by four wires, .91 m in length, attached to the top plate of the generator. It hangs in the hole in the baseplate between the bumpers. The plate is positioned such that in a free state, the distances between the points of contact of the bumpers and the droplet generator are equal. Proper adjustment is necessary to ensure that the motion of the generator is not biased to one particular bumper.

A mechanical energizing arm is used to provide a periodic deflection to one of wires by which the droplet generator hangs. This is

necessary to keep the motion from decaying and to minimize the chance of the motion falling into a particular pattern. The arm is rotated by a motor connected to one end of the arm.

The shape of each bumper is identical. The optimum shape of the portion of the bumper which contacted the droplet generator was determined by experimenting with different shaped inserts which could be screwed into the basic bumper shape of a smooth circular arc. A circular sawtooth design, as can be seen in Figure 3, provided the most uniform distribution and most sustainable motion. A typical droplet distribution is shown in Figure 4.

Electrical power to the solenoids is provided by the same power supply and relay as that used for the water droplet generator. All three solenoids are connected in parallel and energized by 14 volts DC. The frequency at which the bumpers are activated is 4 Hz.

2.4 Radiant Panels

Three radiant panels are used to simulate the heat environment encountered in a true fire situation. All three panels are conical in shape and capable of temperatures in excess of 700 °C. They may furthermore be approximated as blackbodies.

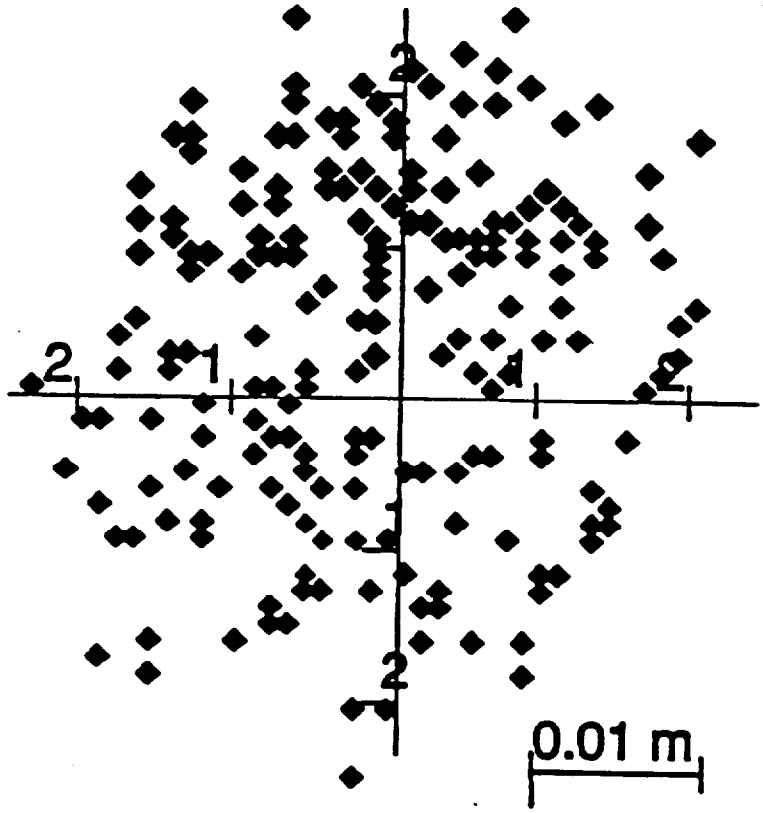

Figure 4 - Droplet Distribution

The design of the panels consists of a rolled, .001 m thick stainless steel housing, formed into a conical shape as in Figure 5. Flexible heater rod, conically wound, is secured to the inside of the stainless steel shell. Cylindrical aluminum mounting studs allow attachment to a suitable holding device.

The panels are connected in a delta circuit and powered by a 208 volt three phase supply. The length and diameter of the heating rod is the same for all three panels, thus they represent equivalent electrical loads. To maintain heater temperature, the panels are placed in a temperature feedback loop, controlled by an Omega CN-7100 digital process controller. This allows the experimenter to enter the desired heater temperature and have it maintained for the duration of experimental runs.

Of the three panels, two are identical in size. These have an external diameter of .2 m and a depth of .08 m. The two equally sized panels are mounted on stands on either side of the macor tile and radiate downward onto the macor surface at an angle of 30° measured from the vertical. The mean vertical distance from the panels to the surface is .159 m. The purpose of these two panels is to provide radiation heat input from above the surface.

The third panel is larger in diameter, at .3 m, with a shallower depth of .07 m. This panel is mounted at a mean distance of .05 m

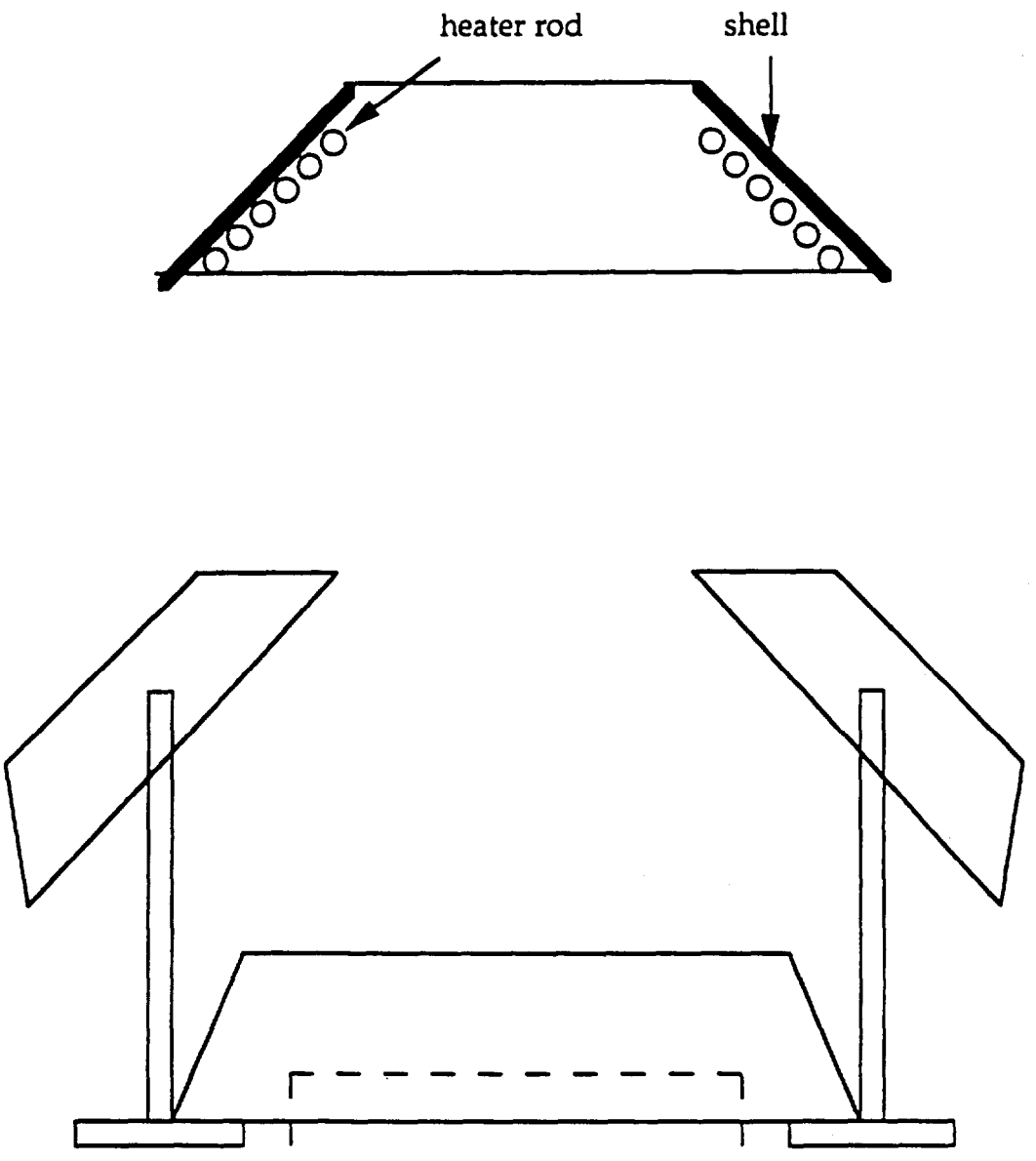

Figure 5 - Radiant Panels

above the macor tile and concentric with it. It surrounds the perimeter of the tile and provides heat input at small angles to the surface and to the sides of the macor. The placement of the heaters is shown in Fig. 5.

The geometry of the heater setup is optimized to prevent any stray radiation from reaching the infrared camera. This is more fully discussed in the Section 2.6, Additional Equipment and Setup Description.

2.5 Degassed Water Dispensing System

A particular difficulty to overcome concerned the dispensing of the degassed water used in the experiment to the droplet generator. Details on the necessity of water degassing and the procedure for doing so are presented in Section 3.1

The droplet generator was originally designed such that the water feed to it was accomplished by attaching the feed line to a reservoir open to the atmosphere. Recall, however, that to maintain control over droplet size, it is necessary to precisely adjust the elevation of the reservoir so that the static head was zero (i.e., when droplets just ceased to fall on their own from the needle tip).

Two problems then become apparent concerning the dispensing of the degassed water to the droplet generator. First, a way is needed to deliver the degassed water to the droplet generator without allowing

it to come into contact with air, as opposed to having a container open to the surrounding atmosphere. Additionally, the system needs to allow precise adjustment of the static head.

To solve the these problems, the water needs to be dispensed from the same container in which it is degassed. A specially designed Pyrex reservoir with a fluid capacity of .2 L is used for this purpose. As shown in Figure 6, the reservoir consists of two sections. The lower section is a large test tube, annealed to withstand high thermal stresses, with a male ground glass joint on the open end. The top portion fits over the lower, and has two valves and a septum connected to it. The septum allows sampling of the water to check for purity during the degas procedure.

To dispense the water to the generator, a mineral oil head control tank works in conjunction with the water reservoir. As also shown in Figure 6, a tank open to the atmosphere is connected by a flexible plastic tube to the top valve of the overturned reservoir of degassed water, under vacuum from the degassing procedure. The head control tank is filled with mineral oil, chosen because of its immiscibility with water, lower density than water, and ease of cleaning from the glass surfaces. To the side valve is connected a .00158 m diameter length of plastic tubing, leading to the droplet generator. When the top valve is slowly opened while keeping the side valve closed, the mineral oil seeps

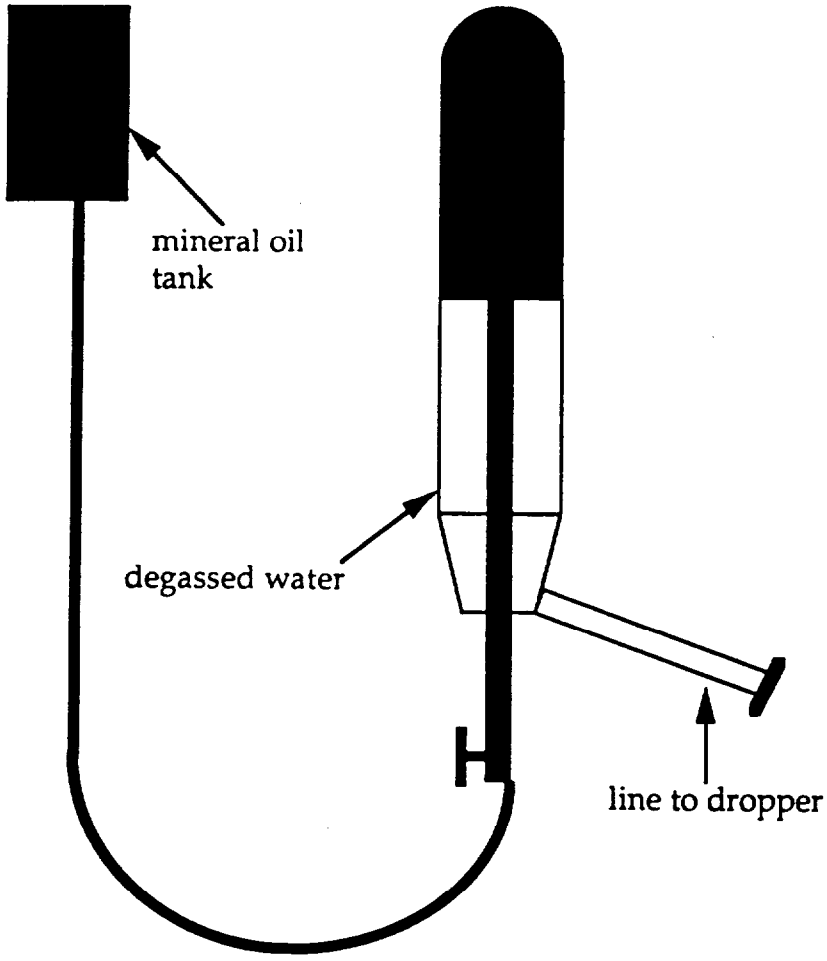

Figure 6 - Dispensing System

through the tubing into the water reservoir and rests on top of the water surface, providing a seal between the water and surrounding air. The amount of mineral oil that the air must diffuse through to reach the water ensures that, over the time of an experimental run, a negligible amount of air is absorbed by the water. The static head can be adjusted with the required precision by adjusting the elevation of the head control tank. Opening the side valve then allows water to flow from the reservoir into the droplet generator.

2.6 Additional Equipment and Setup Description

Details of the remaining equipment and experimental setup depicted in Figure 1 will now be discussed.

The material used for the heated surface is macor, a glass like ceramic able to withstand high thermal stresses. It was chosen because of its relatively low thermal conductivity (1.29 W/m°C) and high emissivity of .84 [6]. The size of the macor tile is (.1524 m x .1524 m x .0254 m). In order to ensure that the initial surface temperature is uniform, the tile is attached to a chill plate using Dow Corning Silicone Heat Sink compound. The chill plate consists of a (.5824 m x .565 m) steel plate with 12 adjacent tube passes running through it. It holds the bottom surface of the macor at an average temperature of 35 °C and establishes a linear temperature profile throughout the solid initially.

Ordinary cold tap water enters on one side at a high flow rate, is circulated through to cool the lower macor surface, and exits from the other side. The temperature of the bottom surface is monitored by a group of five symmetrically placed Omega Chromel-Alumel thermocouples connected to an Omega digital temperature readout.

Of extreme importance is making certain that stray radiation or reflected radiation from the heaters doesn't reach the infrared camera, since the only radiation which has physical meaning for the determination of the surface temperature is that which comes directly from the surface. A careful arrangement of the radiant panels with a chill pipe device is used to accomplish this. The chill pipe consists of two concentric brass pipes, each .508 m in length and .0925 m and .1143 m in diameter, held together by end caps to form an annular flow channel. Water exiting from the chill plate enters the pipe through a fitting on the top and circulates through the annular region before exiting on the bottom. The inside of the pipe is painted flat black. With proper selection of pipe length, diameter, and angle to the surface, unwanted radiation which enters the chill pipe at the bottom strikes the cool, black inner wall and is absorbed. A geometric analysis was carried out which considered the most extreme case for stray radiation leaving the radiant panels, reflecting from the macor surface, and

reaching the camera. This determined the most suitable dimensions of the pipe and the placement of the pipe and heaters.

An aluminum heat shield is used to isolate the droplet generator positioning plate and main dropper body from the heated environment. On the top, or cool side of the shield are mounted two small fans which force air over the positioning plate and dropper to aid in cooling.

The primary data acquisition instrument, an infrared camera, is positioned at the top of the chill pipe and is aimed down through it to focus on the macor surface. Details on the infrared camera and data acquisition system will be discussed in Section 4.

3. EXPERIMENTAL PREPARATION AND PROCEDURE

The primary parameters being varied in the experiments were the mass flux of the water impinging on the surface and the initial surface temperature. In order to ensure equal heating conditions, experiments at three different mass fluxes were run at the same initial surface temperature in one experiment session. Five temperatures were studied with three mass fluxes at each. These temperatures were 111°C, 131°C, 151°C, 162°C, and 182°C. Preparation of the materials and equipment used and the experimental procedure is now presented.

3.1 Water Degassing

To obtain the most meaningful physical insight into the evaporation phenomena, it is essential that a pure fluid be used. This means that the water used in the experiment had to be free of any dissolved minerals and condensed gases normally present in "ordinary" tap water. Results of experiments using only degassed water are especially important since they form a reference set of data to which experimental results using gaseous water may be compared.

Water, however, presents difficulties in that it is particularly susceptible to the absorption of condensible gases found in air. Therefore, it is necessary to somehow remove these gases from the water before it can be used in the experiments. A method known as

"freeze-vacuum-thaw" was used to accomplish this. This procedure relies on consecutive cycles of freezing, vacuum pumping, and thawing the water to remove the gases, and is executed as follows.

A .15 L volume of distilled water is held by the Pyrex reservoir described previously concerning water dispensing and shown in Figure 6. To create a tight seal and provide good vacuum, Dow Corning High Vacuum Grease is used to couple the two sections of the reservoir. The valve extending out of the top of the reservoir is kept tightly closed and unused for this operation. A Welch Duo-Seal vacuum pump is connected to the valve protruding from the side of the reservoir. As this valve is opened to vacuum, the reservoir is immersed into a dewar of liquid nitrogen, freezing the water inside while simultaneously pumping off the head. This process continues for approximately 15 minutes, after which time the valve is closed and the reservoir then placed into a warm water bath to thaw the water. Upon thawing, liberated gases migrate into the evacuated space above the water surface and are pumped off in the next cycle.

A septum on the reservoir allows the water to be drawn by a hypodermic needle and checked for remaining gases without degrading the vacuum in the reservoir. To test the water, a droplet is placed on a smooth aluminum surface at 96°C and observed for gas bubbles. At this temperature, water is still in the evaporation phase of vaporization,

so any bubbles present must be dissolved gases other than water. When bubbles are no longer seen, the water is considered sufficiently degassed. Twelve cycles are required for the amount of water used in these experiments.

3.2 Surface Preparation

The macor surface is cleaned between runs with ethyl alcohol. After the remaining alcohol is evaporated from the surface by heating, it is lightly rinsed with distilled water and allowed to dry.

3.3 Electronics and Heater Warmup

Electronics are allowed to warm up at least two hours before experiments are initiated. This is especially important for the infrared camera and its associated control unit, which have a tendency to drift when just turned on. These details are discussed more fully in the Data Acquisition section. Additionally, the power supply is given at least an hours warm up and the relay at least 15 minutes.

To allow the surface to reach the desired initial temperature, the radiant heaters are turned on at least two hours before experiments are initiated. This amount of time is necessary to allow the heaters to stabilize to the temperature set on the process controller, and most importantly to allow the temperature of the macor tile to reach a steady

state. The surface temperature is monitored with an Omega surface thermocouple probe (chromel-alumel metals) which is placed on the surface prior to heating and remains there until the experiment begins, ensuring adequate time for equalization of the thermocouple and surface temperatures.

3.4 Droplet Size

Droplet size is checked before every experiment. To do this, the droplet generator is turned on and run for approximately 10 minutes in order to allow the system to stabilize. After this time, 50 water droplets are collected in a beaker, which is then quickly capped to avoid evaporation of the water. A Metler electronic balance is used to mass the water droplets and beaker, and care is taken to keep the balance turned on between readings to ensure a consistent calibration.

3.5 Mass Flux

After the droplet volume is adjusted and determined, the frequency of the relay connected to the droplet generator is set to provide the desired mass flux. The expression for the mass flux is given by

$$G=\frac{\rho Vf}{A_w} \quad (1)$$

where ρ is the density of water, V is the droplet volume, f is the droplet generation frequency (Hz), and A_w is the wetted area. To determine the wetted area, a parameter determined once and taken as the same value for all experiments, water droplets are collected over the time of an experimental run on a piece of aluminum foil covered with chalk and with a slight cup shape. The chalk gives a clear indication of where the droplets land, and the slight cup shape makes certain that the water droplets run down toward the center of the wetted area, indicating the outer circular perimeter of the wetted region. The average wetted area used in the experiment is .000033 m^2.

At approximately ten minutes before a run is initiated, the droplet positioner is turned on and motion of the droplet generator begun. This allows time for the solenoids on the positioner to warm up and the motion to develop.

When all of the above procedures are completed, experiments are started. For each run at a given mass flux, the droplets are allowed to impinge on the macor surface for a period of twenty five minutes. Over this time, the real time image from the infrared camera is recorded onto 8 mm videotape, which is then analyzed at a later stage to obtain the desired data. Between each run at a given mass flux, the surface is

given time to recover to the initial surface temperature, as checked with the thermocouple probe. At the end of a set of runs, the image from the videotape is then processed to obtain temperature information about the surface. The complete details of the data acquisition system will now be described.

4. DATA ACQUISITION SYSTEM

The data acquisition used in the experiments represents a novel approach to temperature measurement for this application, and its successful setup and utilization formed a major part of the study. The details of the configuration are shown in Figure 7. Discussion of the individual components shown in the figure now follows.

4.1 Infrared Camera

The first and critical link in the various components comprising the system is the infrared camera. This device detects infrared radiation in the wavelength range of 8 μm to 12 μm and provides a real time gray scale image of the temperature patterns in the target object. In the image, often referred to as a thermograph, darker portions correspond to cooler regions of the target and the lighter portions to hotter regions. Actual radiation detection is accomplished by means of a liquid nitrogen cooled semiconducting material housed in the camera.

Temperature measurement by these techniques is referred to as infrared thermography. In previous efforts of the same research program, Klassen [6] successfully used infrared thermographic methods in the study of single droplet evaporation, followed by Kidder [7] who further studied single droplet evaporation under conditions of radiant heat input.

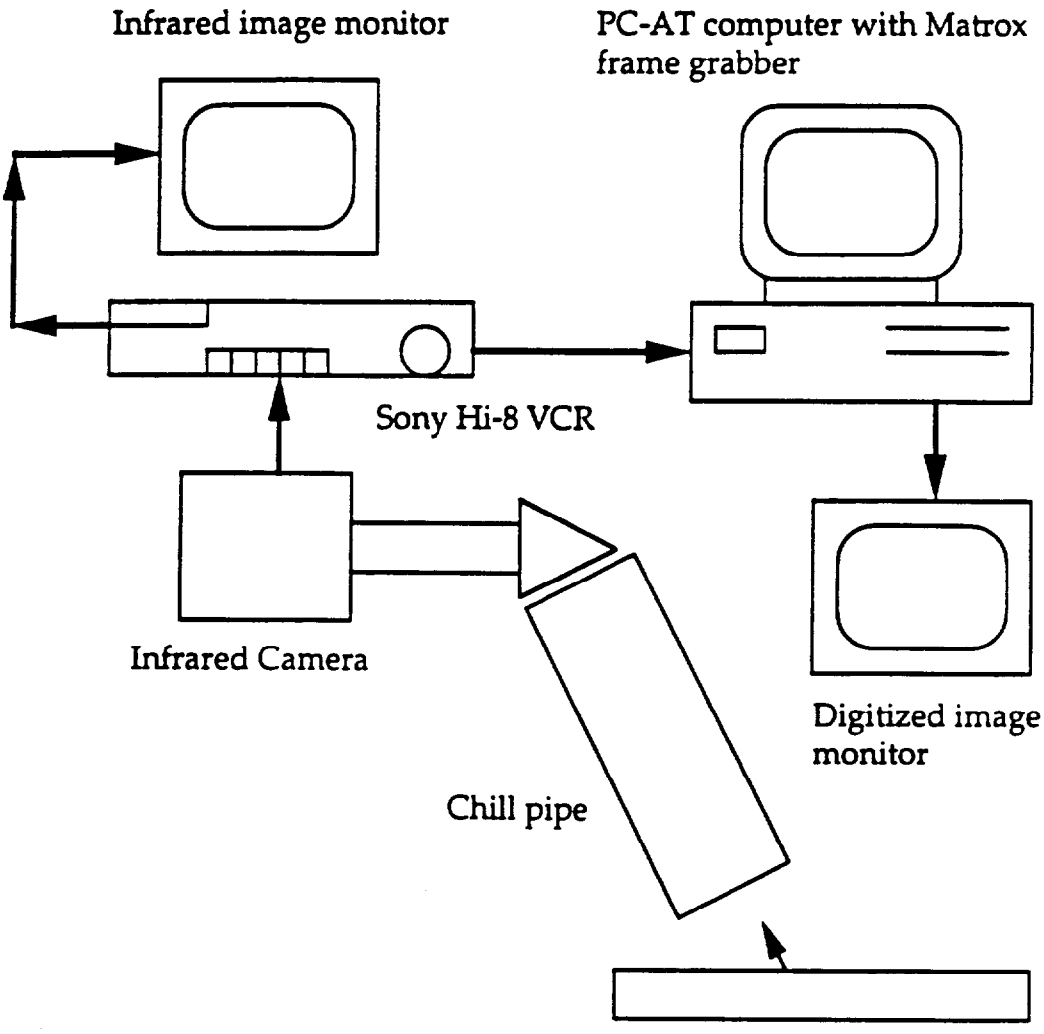

Figure 7 - Data Acquisition System

One of the greatest advantages in using an infrared camera for temperature measurement lies in the fact that it is a non-intrusive, non-contact instrument. Thermocouple devices, because of placement considerations, often disturb the system being observed, and their response is subject to their thermal time constant. In an experiment such as this one, thermocouples couldn't be placed on the surface, as this would have completely intruded upon the radiation field and phenomena being studied.

The camera used in this study is an Inframetrics Model 525. It is mounted on a swivel stand connected to a height adjustable jack, which allows full control over the camera position. A .61 m focal length close up lens is used because of the close working distance between the camera and the surface, and a 90° bending mirror is attached to the end of the lens to facilitate aiming the camera at the surface. A JVC monitor is connected to the camera in order to view the image. The principle of operation of the camera necessitates cooling by liquid nitrogen, requiring close watch of the liquid nitrogen level and refills at intervals of no more than 1.5 hours. If the liquid nitrogen becomes depleted, the camera ceases to function properly.

Operation was similar to that of a conventional movie camera, with control over the focus and field of view. In all of the experiments, the field of view is the same and corresponds to a viewed region on the

surface of (.0075 m x .0055 m). This area is determined by viewing an object of known dimensions and them measuring the size of the object on the camera monitor to determine the scaling between the actual size of objects and the viewed size.

4.2 Video Recorder

The image from the infrared camera is recorded on to 8 mm videotape using a Sony Model S900 Hi-8 video recorder, the next component in the system. Using the Hi-8 format gives increased resolution and picture quality over conventional 8 mm recorders. Recording the image allows a complete thermal record of the macor surface to be permanently stored for future analysis.

4.3 Frame Grabber

The final component in the data acquisition system is a personal computer with a frame grabbing board housed inside. Frame grabbers are hardware devices which can digitize a single frame of a moving picture, where one frame time equals 1/30 of a second. Images can be digitized into a specific number pixels, the fundamental unit of spatial measure in a video display, and into a discrete number of gray shades, typically a power of 2 (i.e. 64, 256, 1024). One of the powers of frame grabbing is that the color, or value, of each pixel in the digitized image

can be accessed directly by the computer and manipulated to reveal information about the image.

A Matrox MVP-AT grabber board is used in this investigation. This is a high speed, high resolution device capable of real time frame grabs. Analysis is assisted by the IMAGER-AT software libraries included with the grabber, which are written in the C programming language and linkable with the user's source code. The grabber is resident in an IBM PC-AT personal computer. An additional monitor is connected to the grabber to view the digitized image.

The system allows infrared images to be sent to the frame grabber, digitized, and analyzed on a pixel by pixel basis. With proper calibration, quantitative spatial and transient information about the surface temperature may be extracted. The methods used to extract this information form the next section.

5. DATA ANALYSIS AND REDUCTION

5.1 Calibration

The capabilities of the data acquisition system make possible a thorough analysis of the temperature behavior of the surface. However, the only information provided by the infrared camera and frame grabber are gray values. Temperature differences between different portions of the surface can be visualized qualitatively, but to obtain actual temperature values, calibration of the system is necessary.

Since it is possible to determine the pixel value at any point on the surface, and hence a qualitative measure of the temperature, a proper calibration should allow the determination of the actual temperature corresponding to the pixel value at each location. The desired end result is a functional relationship between the surface temperature and the gray value, or intensity, at a given point.

The first step in obtaining a temperature-intensity relationship (T vs. I) for macor is the calibration of the infrared camera using a blackbody source to yield a similar relationship for the blackbody. This is done by recording the infrared image of a Mikron blackbody source over a range of temperatures, and then digitizing and summing over the pixels at each temperature (a technique to be described in more detail shortly) to obtain an average pixel value. This average value is then

plotted against the temperature. The result is represented graphically in Figure 8., and is given by

$$I_b = .981 T_b + c \tag{2}$$

Two different temperatures are chosen from the blackbody calibration, and the macor surface is then viewed at these temperatures and average pixel values obtained for the macor, yielding for the blackbody and macor the following linear relationships

$$I_{1b} = .981 T_{1b} + c \tag{3}$$

$$I_{2b} = .981 T_{2b} + c \tag{4}$$

$$\Delta I_b = .981 \Delta T_b \tag{5}$$

and

$$I_{1m} = c_m T_{1m} + b \tag{6}$$

$$I_{2m} = c_m T_{2m} + b \tag{7}$$

$$\Delta I_m = c_m \Delta T_m. \tag{8}$$

Equating the expressions given in (5) and (8) for the intensity difference yields the following for the slope of the macor line

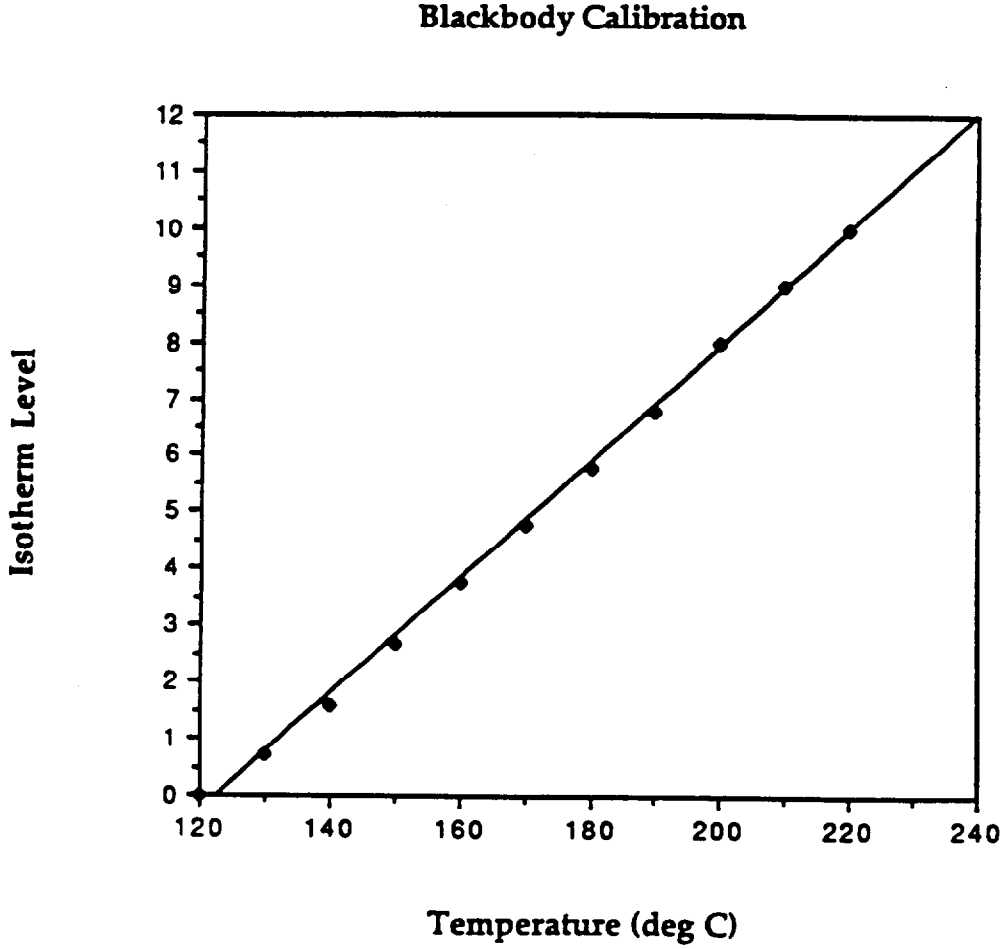

Figure 8 - Blackbody Calibration

$$c_m = \frac{.981 \Delta T_b}{\Delta T_m} \tag{9}$$

For the values used in the calibration, c_m = .858. The desired relationship between the temperature and the intensity of the macor surface is then obtained as a linear function

$$T_m = 1.165 I_m + b \tag{10}$$

The intercept b is determined for each experiment at a different temperature by averaging the pixels of the image of the surface at a certain initial temperature before water starts dropping and simultaneously measuring the initial surface temperature with a thermocouple probe. Inserting these values into (10) provides the T vs. I relationship for a particular initial temperature.

It was initially thought that the presence of the thermocouple surface probe might introduce an uncertainty in the initial temperature measurement, and hence calibration, since the region that the probe reads the temperature of is shielded from incoming radiation. To determine the effect that this had, the probe was placed on the hot surface, viewed with the infrared camera and then quickly removed. The surface without the probe was then viewed at the same temperature. Both processes were recorded and digitized. An average pixel value was obtained for the surface without the probe by summing over the pixels in the digitized image. The pixel locations of the probe

tip covering the surface were determined by examination of the digitized probe image. Then, the digitized frame immediately following the removal of the probe was examined at the same pixel locations to determine if the pixel values under the probe were different than the average pixel value of the surface. Since the time between consecutive frames is relatively short (1/30 second), it is reasonable to assume that the pixel values at the location of the probe obtained from the frame after its removal are the same as those under the probe. Differences between pixel values under the probe and of the rest of the surface would signify a temperature difference between the regions, and thus shielding by the probe. Examination revealed that the variation in pixel intensity was no more than two shades of gray, considered to be within the error of the experiments and therefore not introducing an appreciable temperature difference. Reasons for such minor differences might be that the actual probe surface is relatively small (.002 m x .002 m) compared to the dimensions of the heated tile, resulting in negligible temperature gradients across probe region.

5.2 Transient Temperature Analysis

The transient behavior of the average surface temperature is obtained by digitizing individual frames at intervals of 30 seconds from the beginning to the end of the run. For each of these frames, the pixels

are averaged using a subroutine included with the frame grabber software and called from the user written program PIXAV, listed in Appendix C. This program averages across 3717 pixels, corresponding to an area of the surface (.05 x .05) m in size. The average pixel value at a particular time is then used in equation (10) to determine the average surface temperature at that time. A decaying exponential curve of the following form is then fit to the resulting data

$$T=(T_o-T_{ss})e^{-t/\tau}+T_{ss} \qquad (11)$$

where T_o = initial surface temperature, T_{ss} = the steady state temperature, and τ = the time constant of the fit. The steady state temperature and time constant are the adjustable parameters in the fit, and are chosen such that an equal number of points fall to the either side of the curve.

5.3 Spatial Temperature Analysis

To obtain the spatial distribution of the temperature of the macor surface at a given time, the pixels in a digitized frame are accessed individually, again using the PIXAV code, and for each pixel a temperature obtained using the expression given by equation (11). The pixel value and its (x,y) coordinates are stored in an ASCII file and then fed into IDL (Interactive Data Language, a plotting program) to generate three dimensional surface plots of the temperature versus area.

5.4 Resolution

The spatial temperature resolution is determined by dividing the dimensions of the actual surface area viewed by the number of pixels in the horizontal and vertical direction. Dividing the area calculated previously, (.075 m x .055 m), by the number of pixels in the horizontal and vertical directions, 512 and 480 respectively, gives an average spatial resolution of .0012 m per pixel.

A total of 130 gray shades are used to resolve an average temperature range of 100 °C. This gives a temperature resolution of .76°C/gray shade.

6. RESULTS AND DISCUSSION

6.1 Transient Results

Graphical results for the transient behavior of the average surface temperature for each initial temperature and mass flux are shown in Figures 12 through 25 of Appendix A. These include both the raw data points as obtained from the previously described analysis and the best fit line for each case. Note that initial temperatures of 111°C, 131°C and 151°C correspond to pure convective boiling. 162°C represents the onset of nucleate boiling, and 182°C full nucleate boiling.

A general examination of the plots reveals important features which can be seen in all of the cases. The most significant is that each case seems to decay to a steady state temperature. The oscillatory nature of the data arises because only a portion of the actual sprayed area is viewed. Therefore, at any time, there may be different number droplets viewed than at other times. All raw data is presented in tabular form in Appendix B.

The best fit curve to the data was obtained by assuming a steady state temperature in equation (11) and adjusting the time constant such that an even distribution of points occur around the fitted curve. It might be expected that at higher mass fluxes, the time constant of the fit would be smaller since the surface is being subject to a greater amount of water impingement, thus enabling more heat removal. The time

constants obtained for various initial temperatures are plotted versus the mass flux in Figure 9. From the data shown, there seems to be little recognizable trend in the behavior of the time constant as a function of the mass flux. This suggests that the dominant time scale in the phenomena is not a characteristic of the spray conditions, but possibly determined by material properties. To investigate this, consider the penetration depth, l, of the solid, given by

$$l=\sqrt{\alpha\tau} \qquad (12)$$

For macor, α may be taken as 5.8×10^{-7} m^2/s. Reading an average value for τ from Figure 10 gives approximately 170 seconds. The resulting value for l using the above values is .01 m, or 1 cm. Now consider the radius of influence of a droplet on the macor surface. This is the radial distance from the center of the droplet of the circular region that is most strongly influenced by the cooling effect of the droplet. A thorough analysis is given in references [4] and [7]. It is known from reference [4] that this radius is approximately 4 times the radius of the droplet on the surface of the macor. This value is about .005 m , or .5 cm, for the droplet volumes used in the experiments. This is on the same order as l, and indicates that the time constant, by its presence in l, may be more dominantly a function of the material than of the impinging mass flux of water.

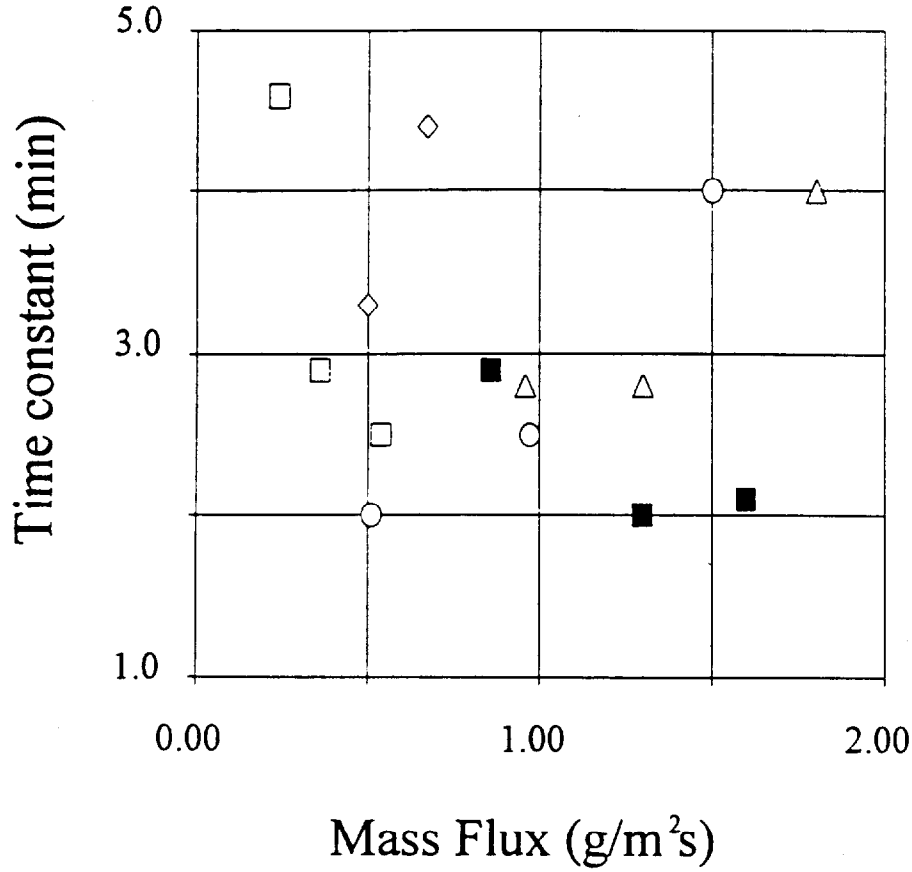

Figure 9 - Time Constant Versus Mass Flux for Various Initial Solid Surface Temperatures (■: To = 182 °C; ○: To = 162 °C; △: To = 151 °C; ◇: To = 131 °C; □: To = 111 °C)

A least squares routine was attempted in fitting the data, but was unsatisfactory because of the inability to include the steady state temperature as a parameter. This method could introduce a possible source of discrepancy in the fits by assuming an incorrect steady state temperature, or by over-representing one part of the data in varying the time constant while under-representing another. An additional source of error would include differences between the actual and calculated mass flux, due to both variations in droplet size and variations in droplet generation frequency because of the time delay relay heating up and falling out of synchronization.

The above discussion suggests the need for a check on the measured results by comparison with an analytical solution. Specifically, an energy balance can be performed on the heated surface at steady state to calculate a steady state temperature and compare it with the measured value. A general energy balance can be written to determine the overall heat transfer coefficient, h, as follows

$$\alpha F \sigma T_h^4 = h(T_o - T_\infty) + \frac{k}{\delta}(T_o - T_b) \qquad (13)$$

The term on the left is the familiar Stefan-Boltzman Law, including the view factor F between the heaters and surface. The first term on the right hand side represents the convective heat transfer from the surface, and the second term heat transfer by conduction through the heated tile,

where δ is the thickness of the tile and k the thermal conductivity. T_o, T_b, T_h, and T_∞ are the initial surface, bottom surface, heater, and ambient (23°C) temperatures, respectively, and α the absorptivity of macor (.84). Solving for h gives

$$h=\frac{\alpha F\sigma T_h^4-\frac{k}{\delta}(T_o-T_b)}{(T_o-T_\infty)} \tag{14}$$

Next, an equation can be written for the overall heat removal from the surface by considering the initial surface temperature and the steady state temperature

$$h_{fg}G=h(T_o-T_{ss})+\frac{k}{\delta}(T_o-T_{ss}) \tag{15}$$

where G is the mass flux, h_{fg} the enthalpy of vaporization of water, and T_{ss} the steady state temperature to be calculated. Solving for T_{ss} gives

$$T_{ss}=T_o-\frac{h_{fg}G}{(h+\frac{k}{\delta})} \tag{16}$$

The overall heat transfer coefficient may be calculated from equation (14) and this value used in equation (16) to determine the calculated value of T_{ss}. This was done, using a measured value of .26 for the view factor F. A plot of the measured steady temperature, as determined form the curve fit, can then be plotted against the calculated value.

Two best fit straight lines to the above data are shown in Figure 10. The line denoted by F corresponds to results obtained using the value .26 for F. As can be seen, small deviations from the desired slope of 1 which corresponds to complete agreement in the measured and calculated temperatures, are visible in the F line. The most spread in the data occurs at the lower temperatures, suggesting a higher steady state temperature than actually measured. This may be due to underestimating the temperature of the surface underneath the water droplets. Underestimation of the temperature would occur because the calibration used to obtain the temperatures is only valid for the macor surface. When the infrared camera records a water droplet which has not yet evaporated, the calibration no longer holds since the camera is seeing the water and not the macor. Approximately 10% of the surface is covered by water droplets at a given time. Taking this percentage of the average apparent temperature drop underneath a droplet, about 40°C, gives an estimate of 4°C by which the average temperature is in error due to this effect. This is a probably a high value, since the region under the droplet is certainly cooler, thus a portion of the 40°C temperature drop is physically meaningful. Additionally, at lower temperatures, flooding of the surface could be occurring, a state where more water is being deposited than can be evaporated. Although the data suggests that some steady temperature is being reached, the

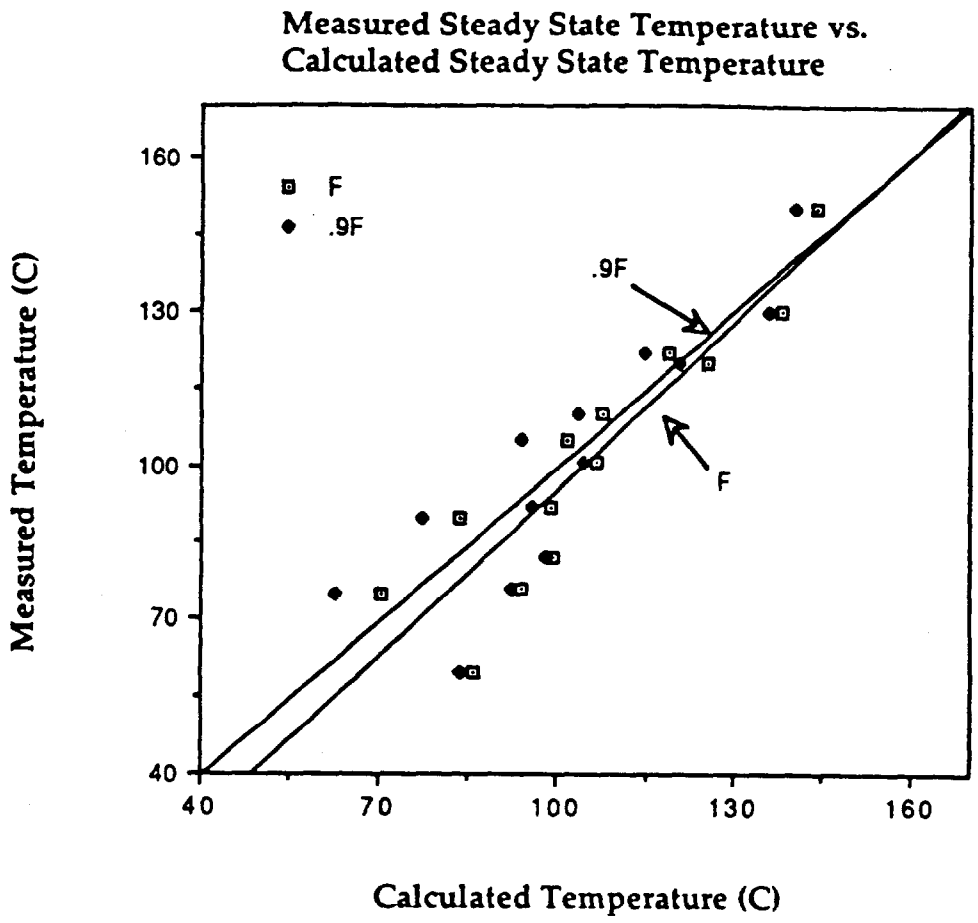

Figure 10 - Measured Versus Calculated Steady State Temperature

evaporation rate may be sufficiently low such that longer time periods are necessary to observe an additional decrease in the temperature.

Another reason for discrepancies would be an overestimation of h. The most significant cause of this would be an error in the view factor used. To assess the effect of this, a temperature difference of 25%, a high value for means of analysis, between the calculated and measured values may be taken and referenced to the ambient (23°C) to give an average normalized difference of 1.1%. Including the ambient takes into account its role as the zero point for the measured temperatures. Mathematically, an expression for the above is

$$\frac{T_{ss,c}-T_{ss,m}}{T_{\infty}-T_{ss,c}} \tag{17}$$

where the subscripts c and m correspond to calculated and measured values. Then, this ratio of 1.1 can be related to the ratio of the different view factors

$$1.1=\frac{F_1}{F_2} \tag{18}$$

where F_1 is the view factor used and F_2 a different value to be determined. Then,

$$F_2=.9F_1 \tag{19}$$

Thus, the temperature difference is related to an 10% difference in the view factor. Taking 90% of F_1 = .26 gives F_2 = .234, and this can then be

used in equations 13 through 16 to obtain the line in Figure 10 denoted by .9F. As can be seen, this gives a result much closer to that which would be expected. For the case of the smaller view factor, the slope is essentially 1, that is, the best fit line shows a strong agreement between the measured and calculated values. To determine the error in spatial measurement needed to cause a 10% decrease in F, an expression for the view factor of a surface located underneath a radiating disc, as shown in Figure 11, can be used to approximate the radiative exchange between the heaters and macor surface, since the bulk of the radiation for evaporation is provided by the heaters mounted above the surface. The following expression is used

$$F=\frac{a^2}{a^2+l^2} \tag{20}$$

where a and l are as shown in Figure 11. Now, equation (19) can be used to determine the variation in one of the spatial dimensions by fixing a = .1 m (measured) in both view factors and letting l = .16 m (measured) in F_1 and solving for l_2 in F_2. This gives l_2 = .168 m. Thus, a difference on the order of just millimeters in a spatial measurement can cause an appreciable difference in the view factor, and hence the calculated steady state temperature. This suggests a likely source of discrepancy in the measured and calculated data.

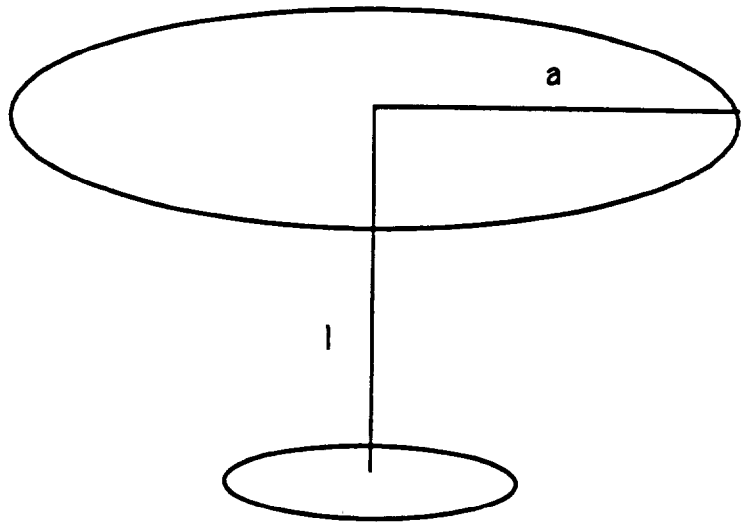

Figure 11 - Geometry for View Factor

6.2 Spatial Results

Surface plots of the spatial temperature distribution are shown in Figures 26 through 39 of Appendix A. These are shown for each initial temperature and mass flux at three distinct times during the transient: 1) very early in the transient, when the surface temperature is close to the initial value; 2) a time well into the transient but before steady state is reached; 3) steady state. Each plot shows a (.05 m x .05 m) area of the macor surface, with temperature indicated on the vertical axis.

The plots provide a qualitative description of the cooling phenomena occurring on the surface at various times during the transient. A trend can be seen in all cases which corresponds to the behavior of the time distribution of the average surface temperature. Consider first, for any instance, the plots at a time very early in the transient. At this time, deep spikes in the surface temperature can be seen. These regions correspond to where droplets have landed on the surface and caused a rapid drop in the temperature. The small fluctuations in the plots are the error associated with the data, and are due to variations in pixel intensities caused by electronic noise and possible surface imperfections. Note, however, that the overall surface in the plots is generally flat at this time, with the exception of where droplets have landed, and very near the initial value. This is explained by the fact that a relatively small amount of water has impinged on the

surface, therefore the effects of the single droplets are more localized and haven't had sufficient time to cause a significant decrease in the average temperature.

At the next time in the sequence, the regions where the droplets have landed are still discernible but are less sharp and tend to run together more. The overall surface is no longer flat, but exhibits a more wavelike shape. This is due to the presence of a greater number of droplets on the surface, causing the cooling effects of adjacent droplets to be superimposed. Additionally, the recovery time for the surface temperature increases as more water is added, resulting in an general decrease in the surface temperature towards a steady value.

The final time in the sequence shows a marked lowering of the surface temperature when compared to the distribution very near the beginning of the transient. At this time, steady state has been reached and the general behavior described in the second time sequence is exhibited to a greater degree. Individual drops become more difficult to localize and the plot surface more wavelike. The net effect is the lowering of the average temperature.

For initial the temperatures of 151°C at high mass fluxes and for runs at 111°C, very low temperatures, at points turning negative, can be seen at later times in the plot sequences. This is due to the previously explained effect of underestimation of the surface temperature.

Additionally, at times late in the transient, evaporation rates are slower and it is possible that more water is present on the surface at a given time, adding to the perceived lower values of the temperature under the droplets. Thus, the plots are more indicative of the qualitative behavior of the surface temperature, and should not be subject to strict quantitative interpretation.

6.3 Accuracy

In addition to the sources of experimental error in the previous discussions, slight variations in pixel intensities due to electronic noise and surface imperfections introduce accuracy limits in the data for both the transient and spatial analyses. The average variation in pixel intensity was ± 2 gray shades, giving an accuracy of about ± 2°C. This can be also be read from the surface plots at times early in the transient, where the surface should be ideally flat, but contains small variations

6.4 Single Droplet Validation

Experiments were also conducted to determine the evaporation time of a single droplet from the macor surface in order to provide a check on the results obtained by Kidder [7]. In experiments over a wide range of initial temperatures, Kidder examined the evaporation times of droplets from 10μL to 50μL. Heat input was provided by two radiant

heaters, and a precision pipette was used to produce water droplets. In addition to evaporation times in the full convective boiling regime, the study found considerably shorter evaporation times in the nucleate boiling regime, as would be expected because of increased flow inside the droplet. Kidder also examined differences between the radiatively and conductively heated surface, and quantified to some extent the effects of droplet impact for the radiatively heated case, an effect to be introduced briefly.

A droplet size of 10 μL was used and the previous results checked at 110°C and 130°C. The evaporation time was determined using the line scan function of the infrared camera. Full details on this function and determining the evaporation time may be found the work by Kidder.

Results are shown in Table 1. Examination reveals considerably shorter evaporation times for the author's results, with a difference of approximately 23% for both temperatures studied. A possible and likely explanation for this may be attributed to droplet impact. When a droplet impacts on a hot surface, spreading of the droplet occurs. This spreading can have a significant effect on the evaporation time. Droplet release height used in this experiment was .3 m, larger than those used in previous single droplet investigations and the cause of greater impact with the surface.

The parameter used to describe droplet impact and spreading is β, the ratio of the radius of the spreaded droplet on the surface to the radius of the droplet modeled as a perfect sphere before impact. The measured value of β in these experiments was 1.61. Kidder found that β increased with surface temperature for the radiantly heated surface, while it remained fairly constant for a surface heated from below. Measured values obtained in his analysis varied from 1.4 to 3.4 over a temperature range of 90°C to 180°C. The increase is explained by the heating of the droplets from above, causing a large absorption of heat by the droplet surface and thus lowering the surface tension which is a function of temperature. The value for this experiment was significantly higher at the temperatures studied as to show a marked decrease in the evaporation time. Avedisian gives an interesting analysis of droplet impact in reference [15].

Analytical results of single droplet evaporation phenomena were obtained by Liao [13], and subject to verification by Kidder's results. The analysis by Liao utilizes an elaborate computer code, and has been validated for the case of single droplet evaporation for both conductive and radiant heat input.

Droplet	Current 110°C Time (s)	Previous 110°C Time (s)	Current 130°C Time (s)	Previous 130°C Time (s)
1	36.6	45.21	22	30.40
2	40.2	45.9	24.6	31.81
3	34.2	46.28	23.6	32.00
4	35.2	46.59	24.2	32.15
5	35	47.42	26	30.59
6	35	46.71	24	33.15
7	34.4	45.53	23.8	29.71
8	38.2	44.84	23.8	29.30
9	32.6	46.34	23	31.12
10	34	46.71	23.6	31.90
Average	35.5	46.15	23.9	31.21

Table 1 - Comparison of Single Droplet Evaporation Times

7. CONCLUSIONS

The spatial and temporal behavior of the temperature of a hot, low thermal conductivity surface cooled by multiple water droplets evaporation was experimentally investigated over a range of different mass fluxes and initial surface temperatures. The span of temperatures studied included both convective and nucleate boiling.

It was found that the average surface temperature decreased exponentially with time until reaching a steady state value. The measured steady state temperature was compared with that determined by an energy balance. The best agreement was obtained by considering a decrease in the measured view factor, which resulted in the smallest differences in the calculated and measured values. Slight variations in the view factor, due to inaccuracies in spatial measurements used to obtain it, can cause an overestimated heat transfer coefficient, resulting in discrepancies. Additionally, a flooding condition may be present on the surface at initial temperatures of 111°C and 131°C, resulting in lower measured temperatures.

It was also found that there is no strong correlation between the mass flux of the impinging water droplets and the time constant of the cooling phenomena. Instead, results suggest that properties of the heated material are the dominant factors in determining the time constant.

The spatial distribution of the surface temperature was also investigated and presented graphically. The results showed a marked decrease in the average surface temperature as steady state was approached and reached. This behavior agrees with that shown in the transient analysis of the average surface temperature, namely the lowering of the surface temperature as the effects of the droplets become less localized at times far into the transient.

Results for single droplet evaporation times were obtained and compared with previous results and found to be lower by 23%. This is explained by considering the effect of greater droplet impact on the heated surface in the present study, resulting in shorter evaporation times due to spreading of the droplet.

A data acquisition system employing the techniques of infrared thermography and digital image analysis was designed and implemented and was shown to be a powerful tool in the field of experimental heat transfer. The methods used gave a high degree of spatial and thermal resolution, and provided a non-intrusive means of temperature measurement.

All results are encouraging in their basic functional behavior and physical consistency. Comparisons have yet to be made with the solution provided by the computer code, as it is still under development for the case of radiant heat input for multiple water droplets.

APPENDIX A - DATA PLOTS

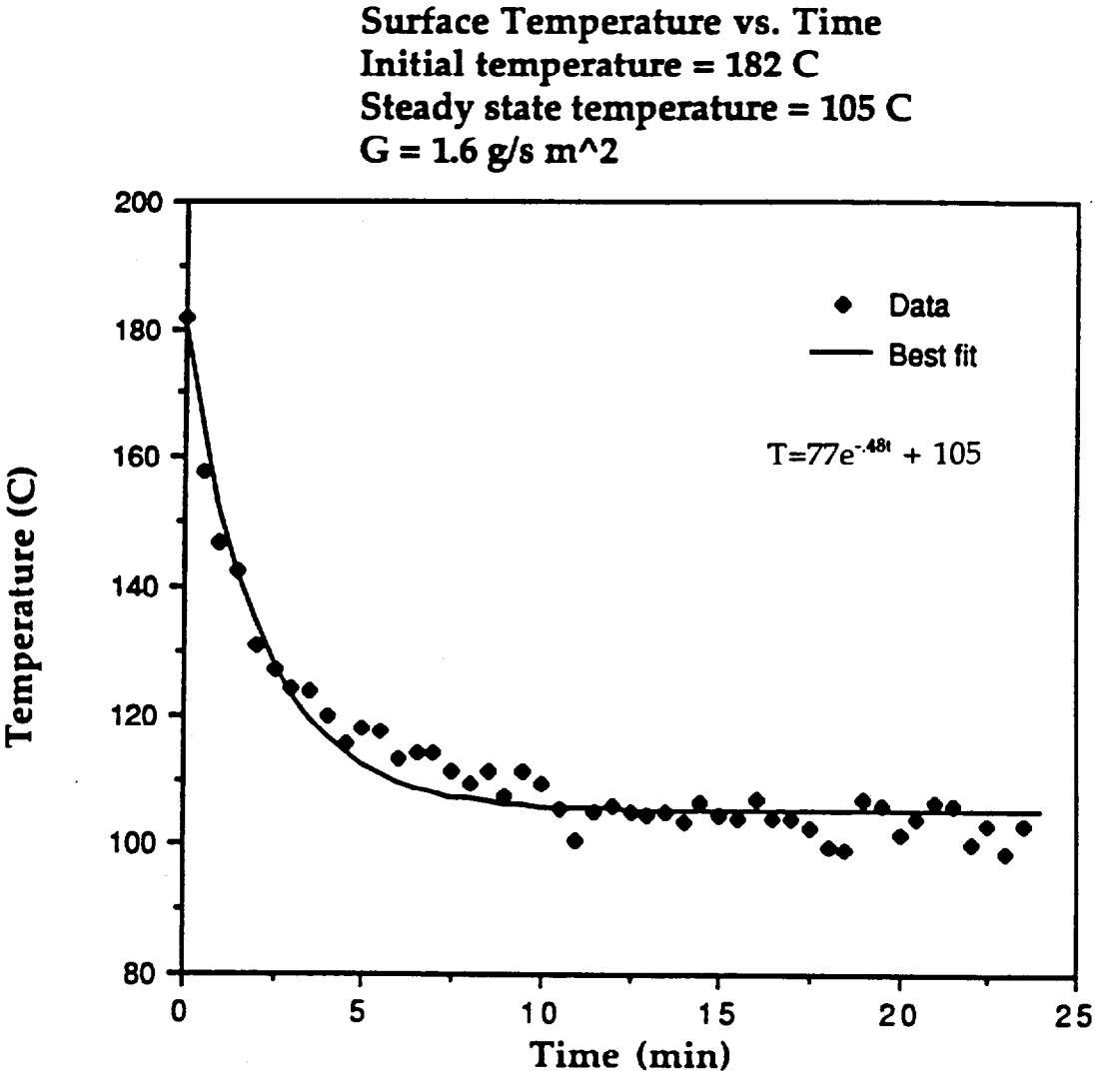

Figure 12 - Time Plot: T_o = 182°C, G = 1.6 g/m^{2}s

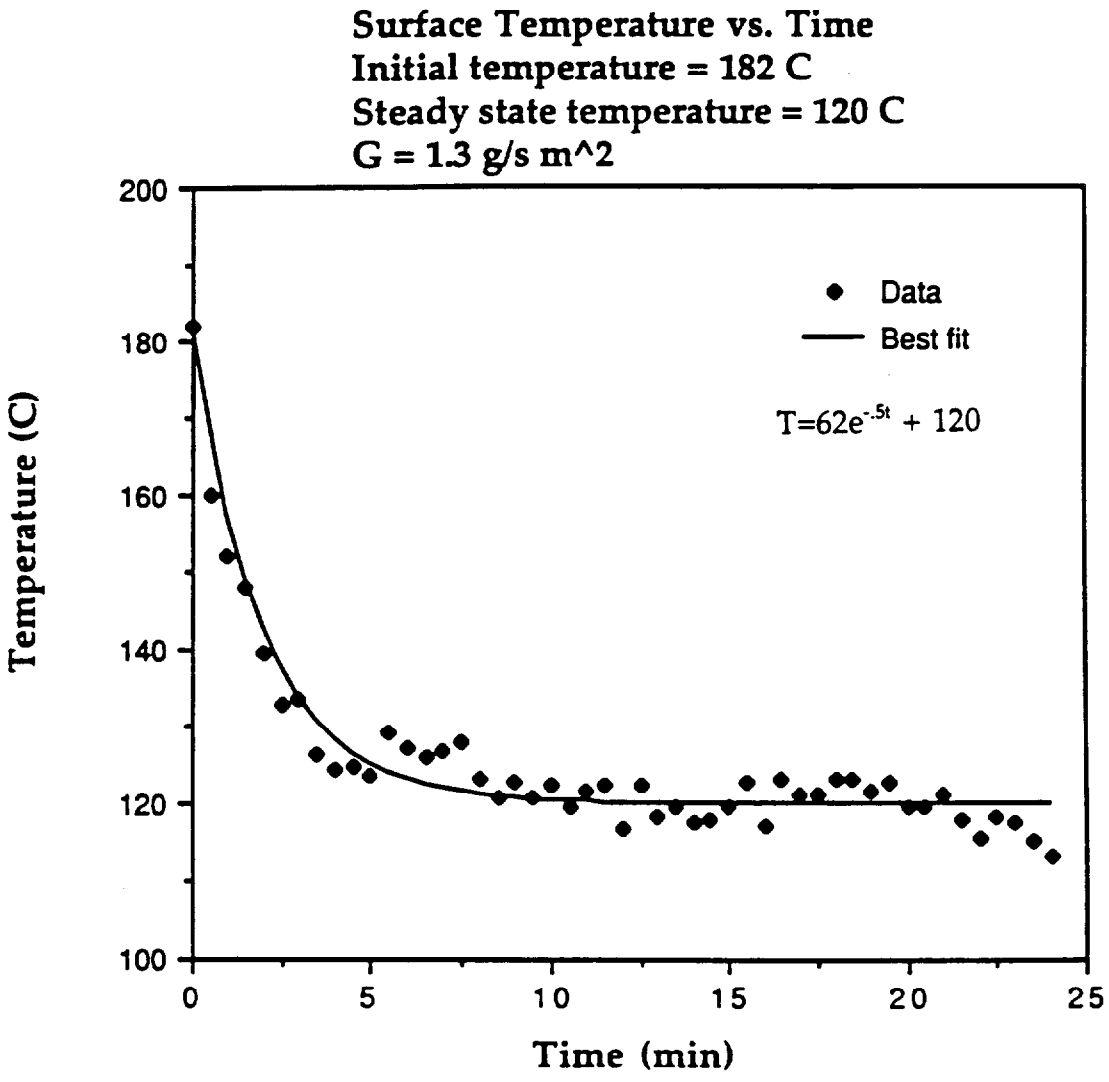

Figure 13 - Time Plot: T_o = 182°C, G = 1.3 g/m^{2}s

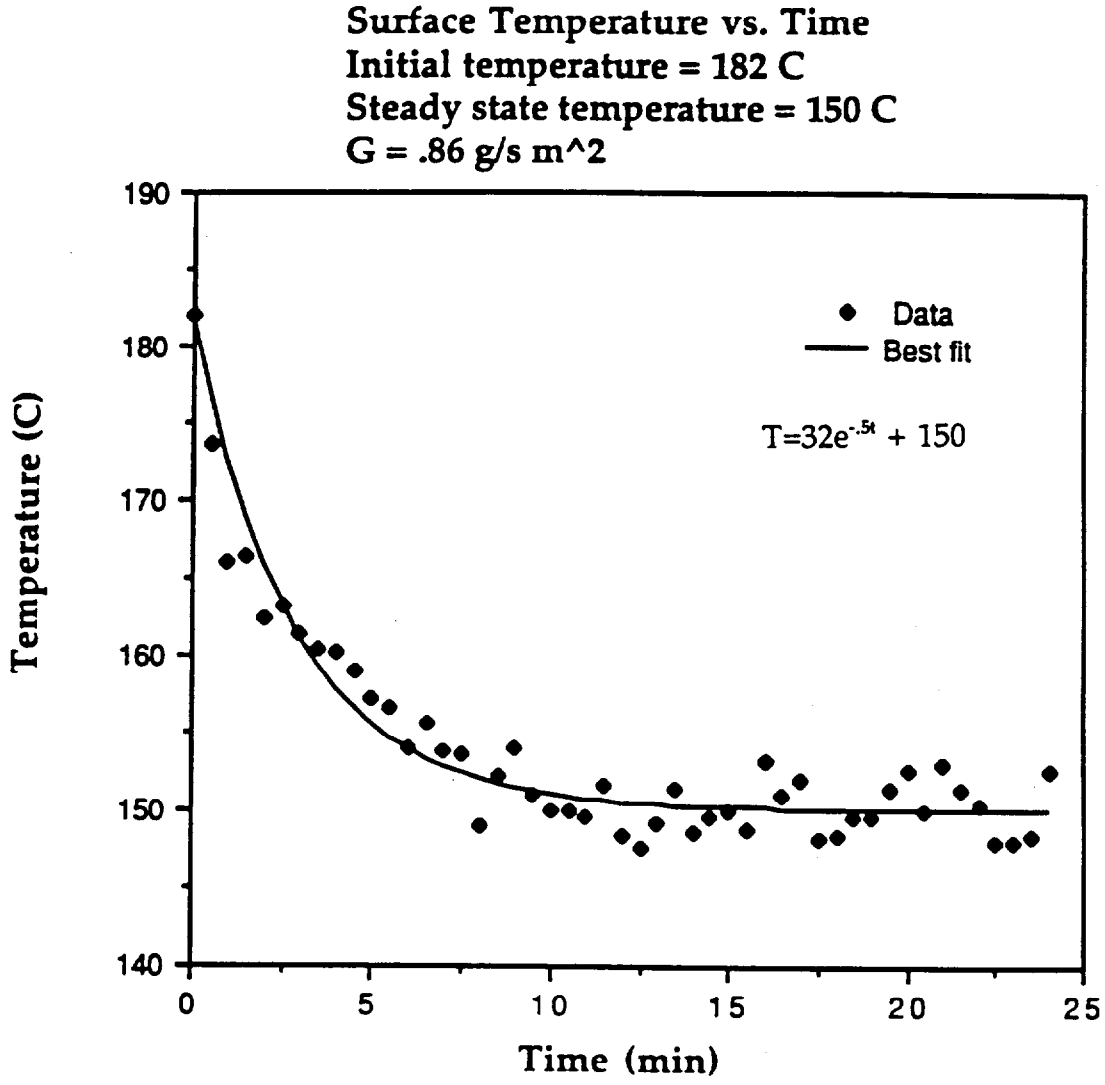

Figure 14 - Time Plot: T_o = 182°C, G = .86 g/m²s

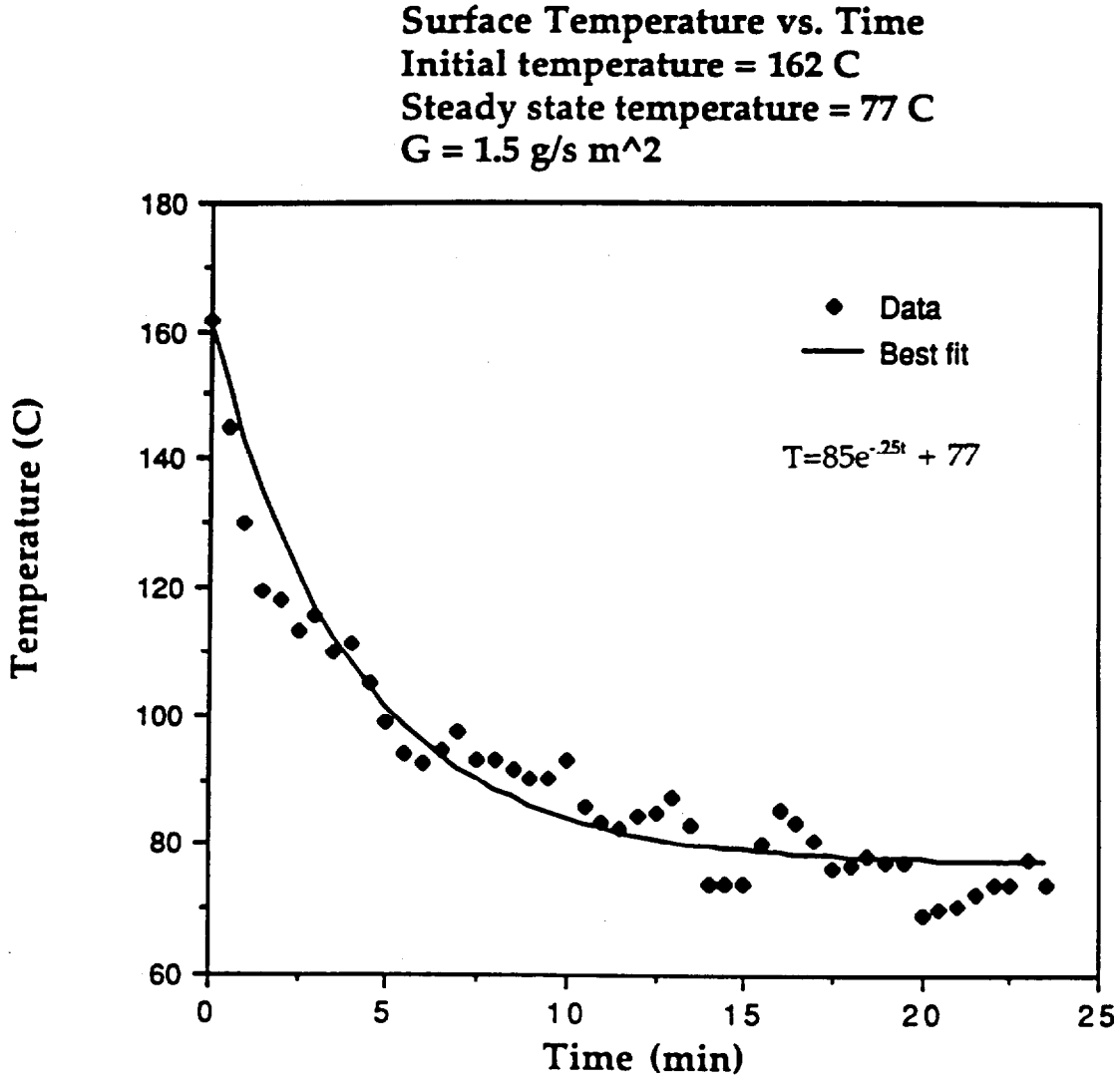

Figure 15 - Time Plot: T_o = 162°C, G = 1.5 g/m²s

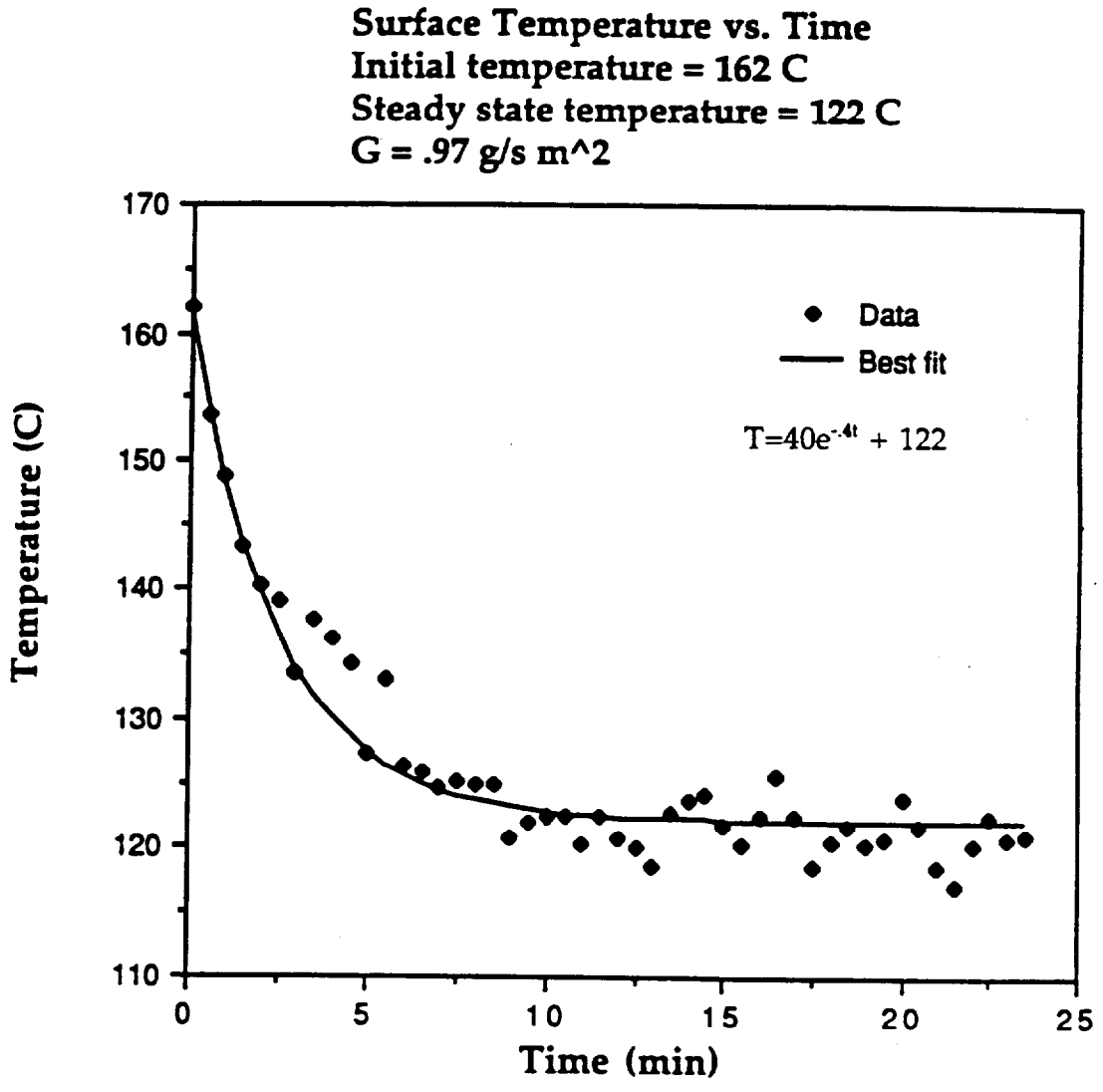

Figure 16 - Time Plot: T_o = 162°C, G = .97 g/m^{2}s

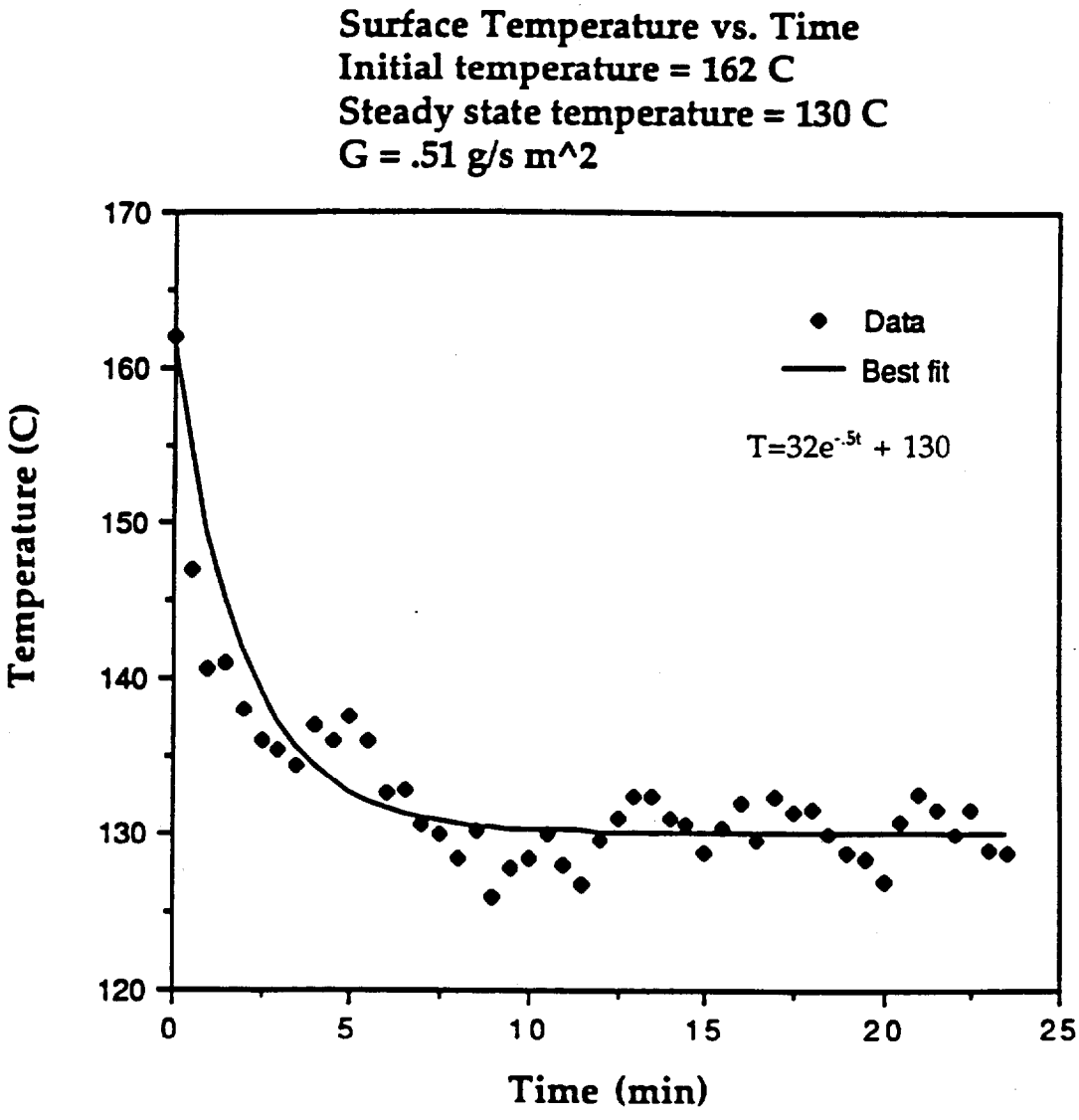

Figure 17 - Time Plot: T_o = 162°C, G = .51 g/m^{2}s

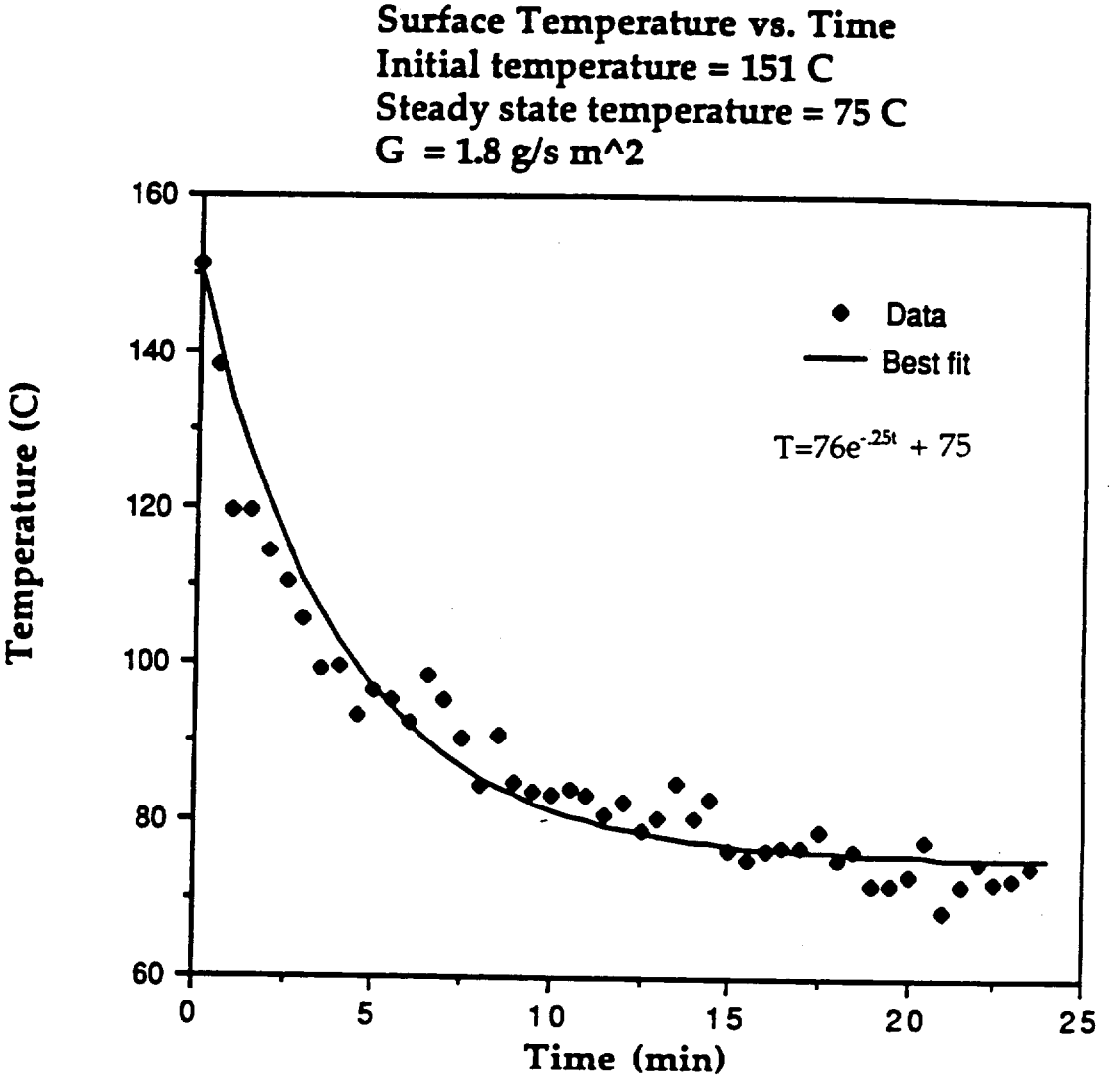

Figure 18 - Time Plot: T_o = 151°C, G = 1.8 g/m^{2}s

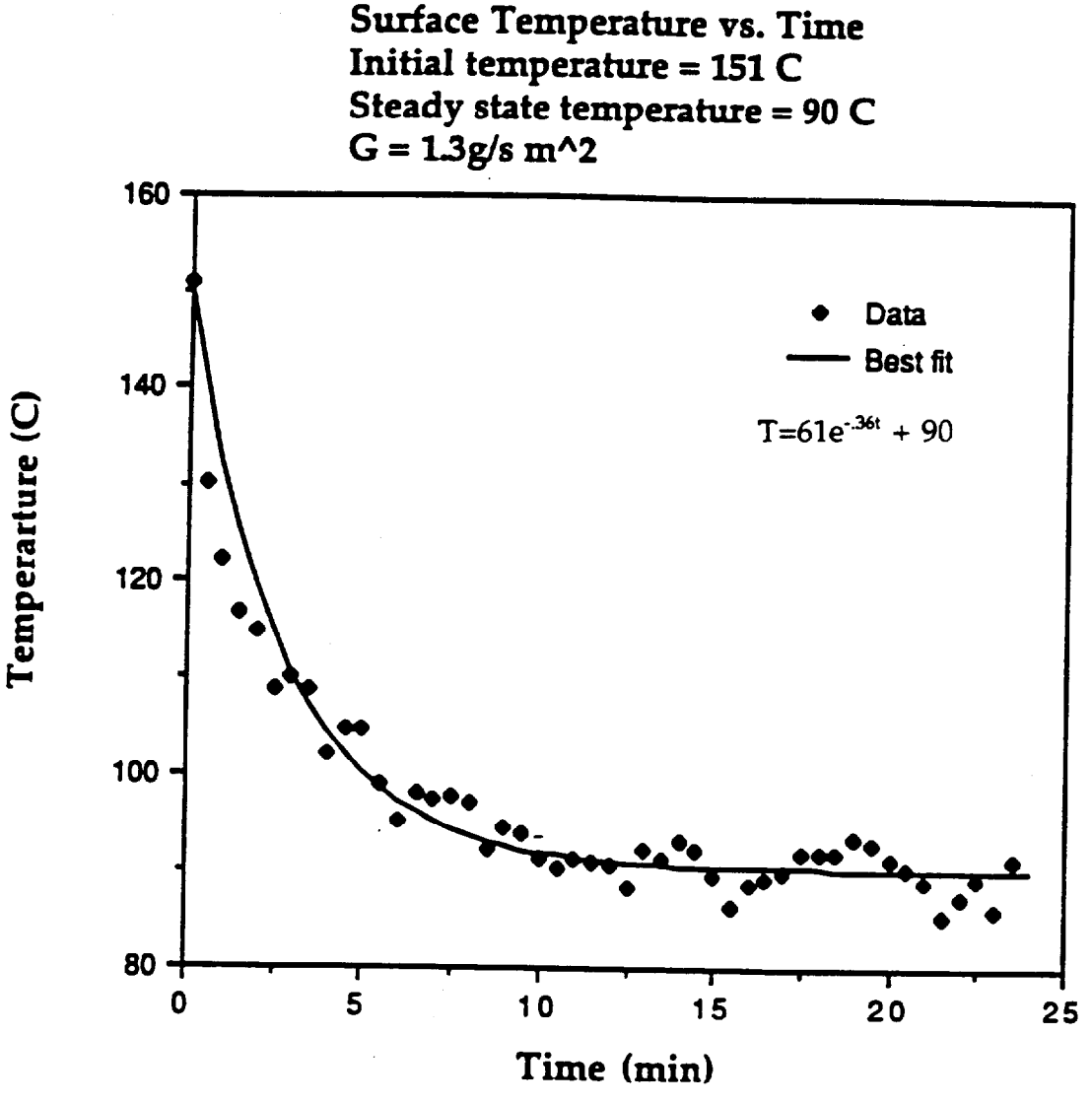

Figure 19 - Time Plot: T_o = 151°C, G = 1.3 g/m^{2}s

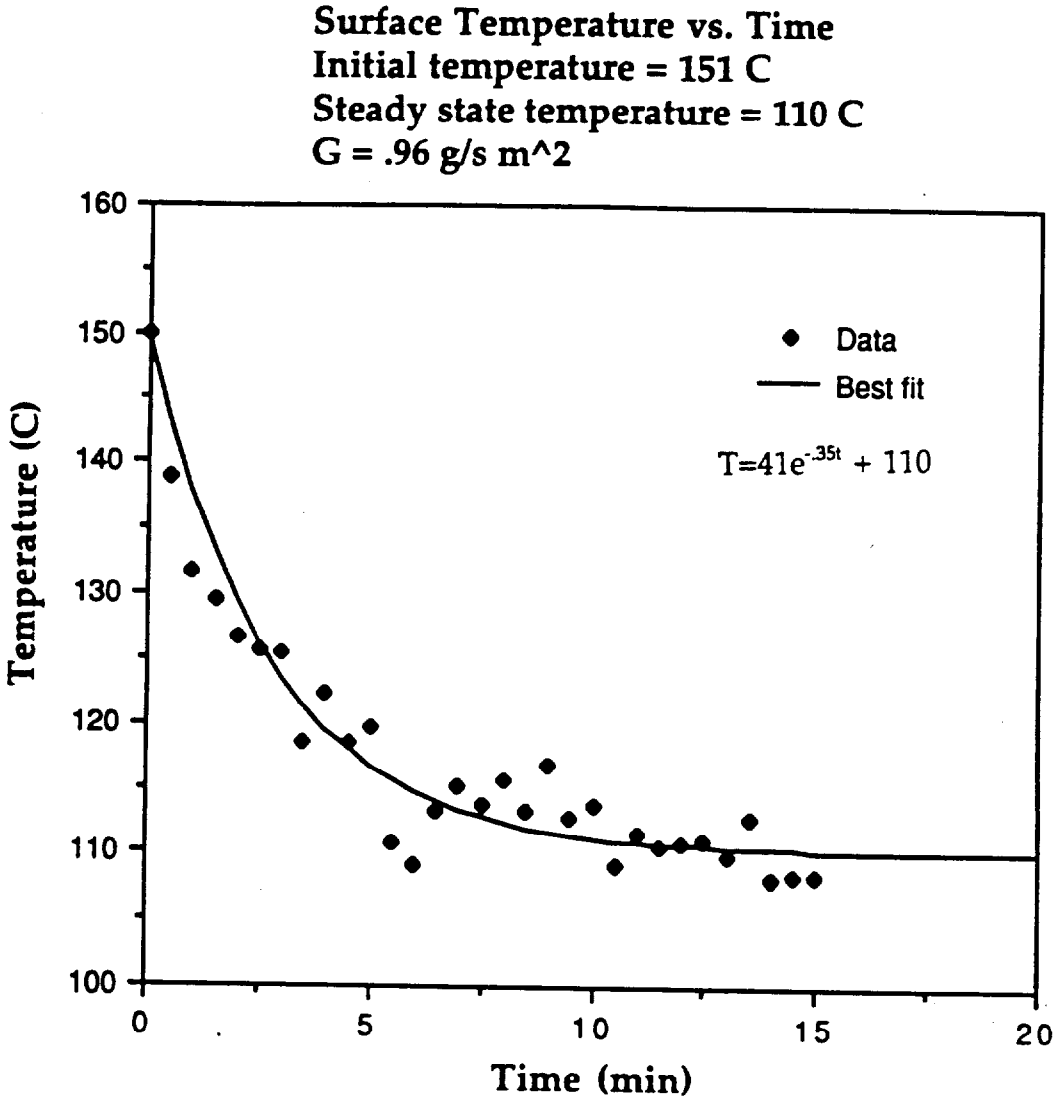

Figure 20 - Time Plot: T_o = 151°C, G = .96 g/m²s

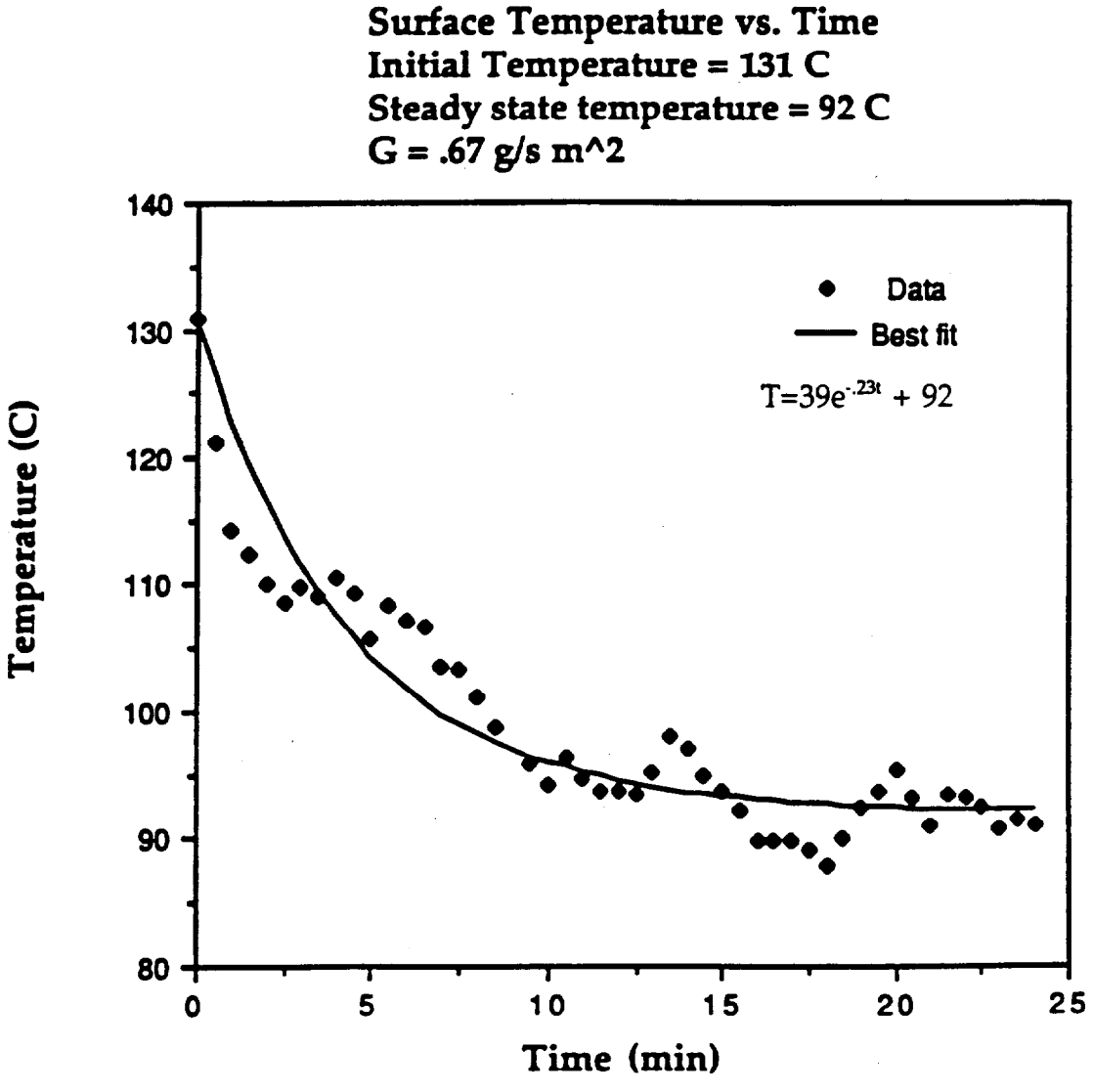

Figure 21 - Time Plot: T_o = 131°C, G = .67 g/m^{2}s

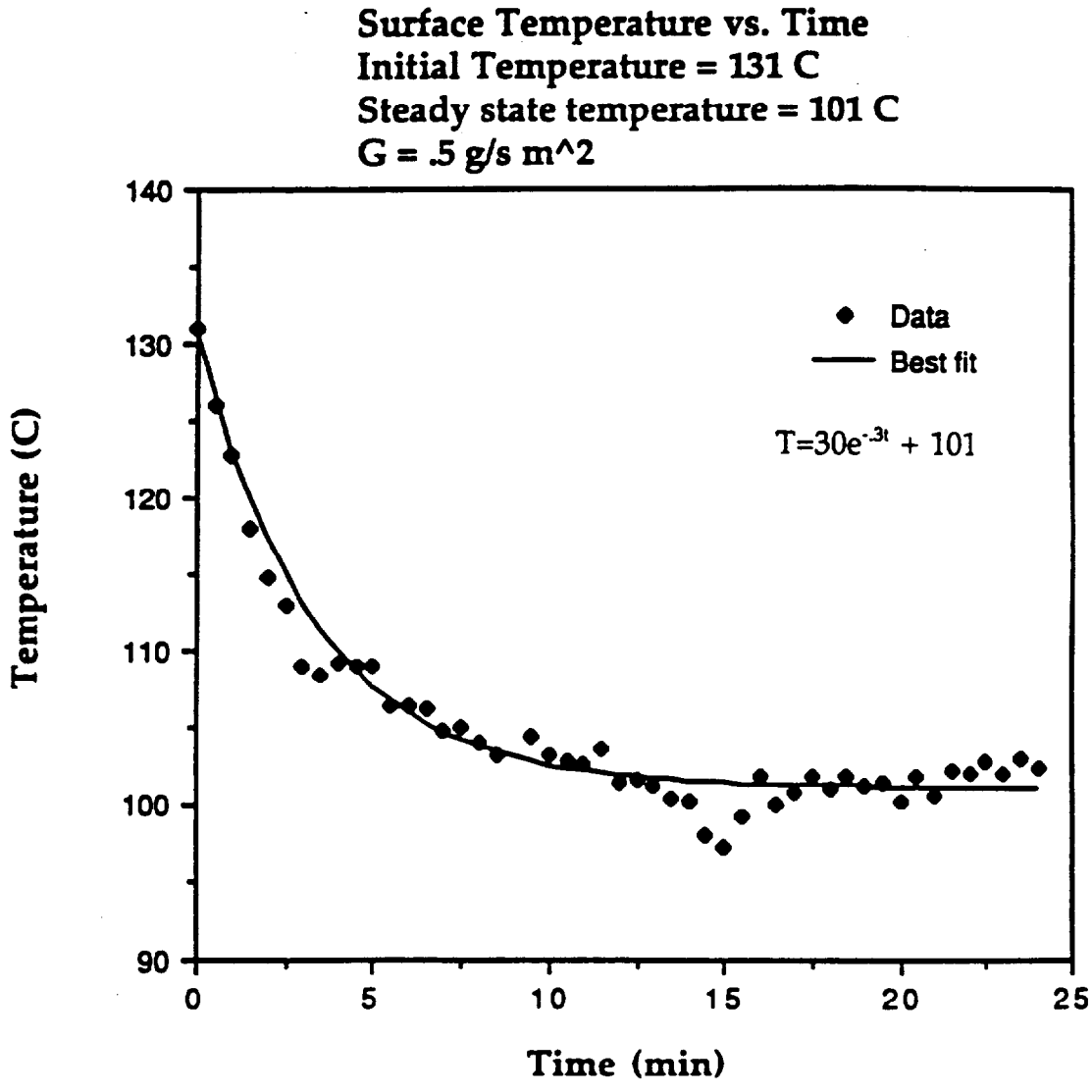

Figure 22 - Time Plot: T_o = 131°C, G = .5 g/m^{2}s

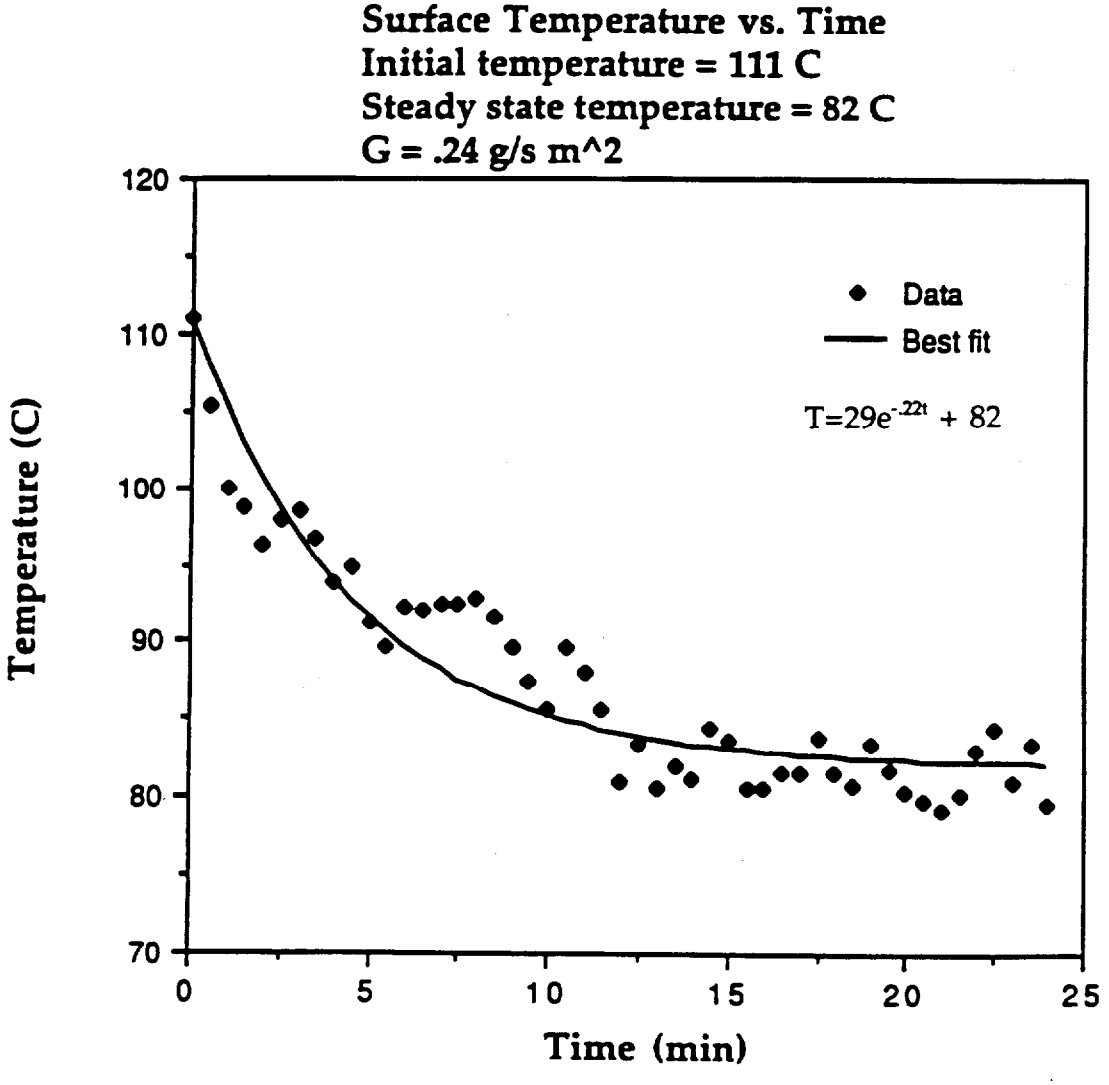

Figure 25 - Time Plot: T_o = 111°C, G = .24 g/m^{2}s

time = 5 s

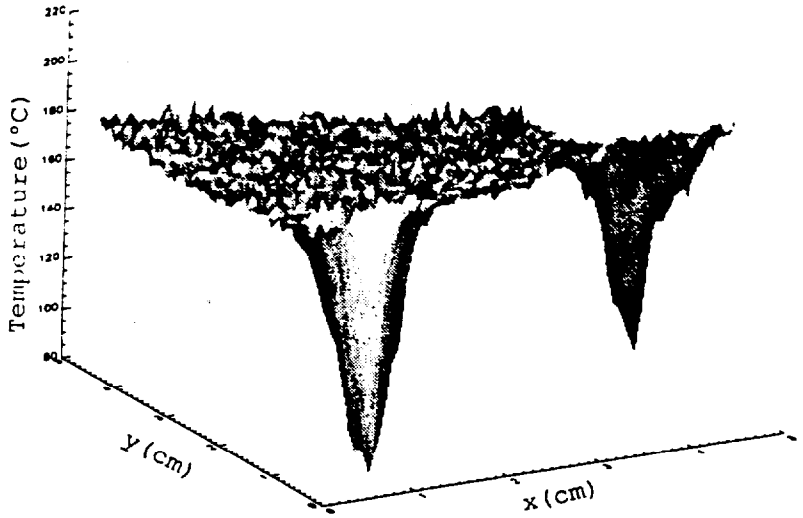

time = 240 s

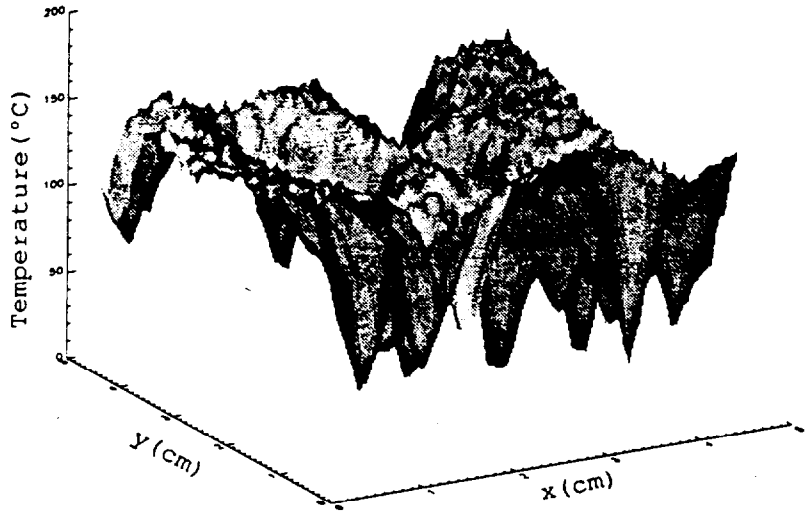

time = 600s

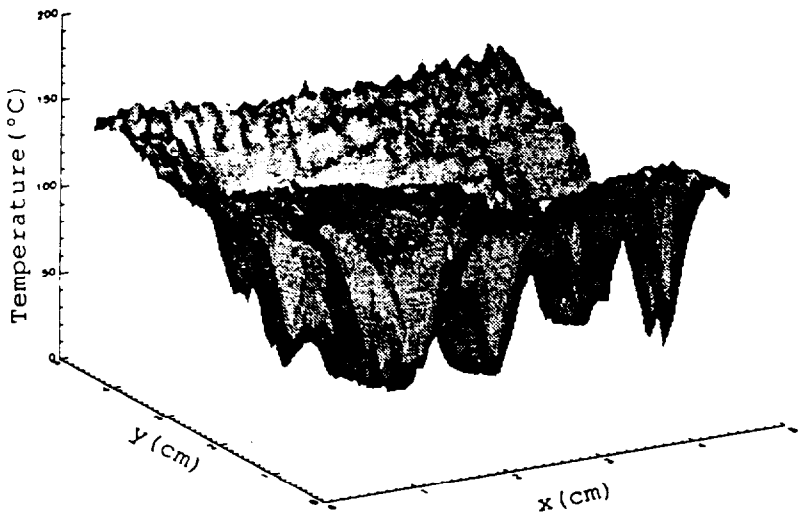

Figure 26 - Surface Plots: T_o = 182°C, G = 1.6 g/m^{2}s

time = 10 s

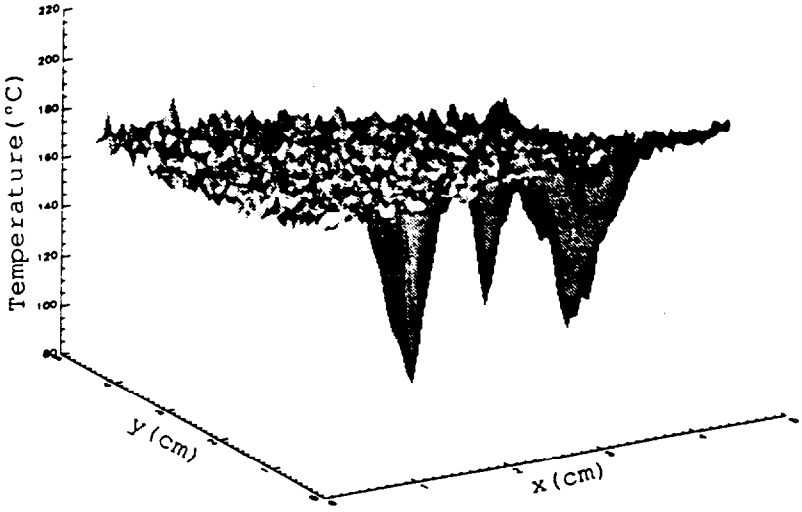

time = 240 s

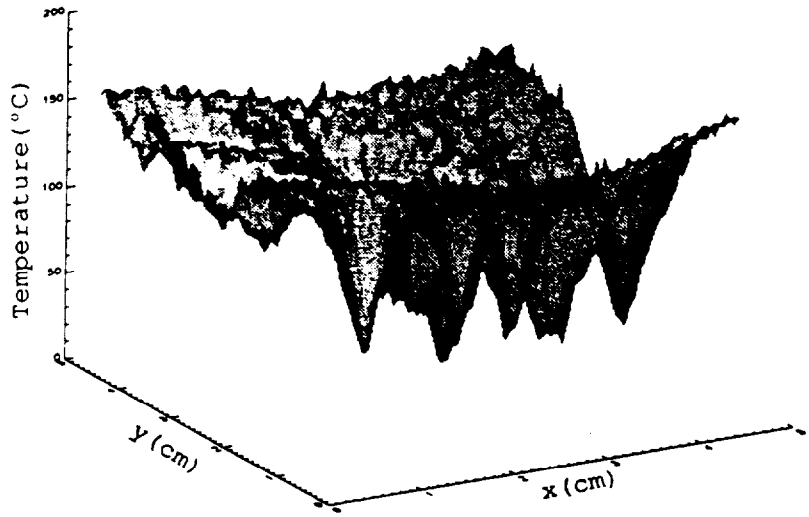

time = 600s

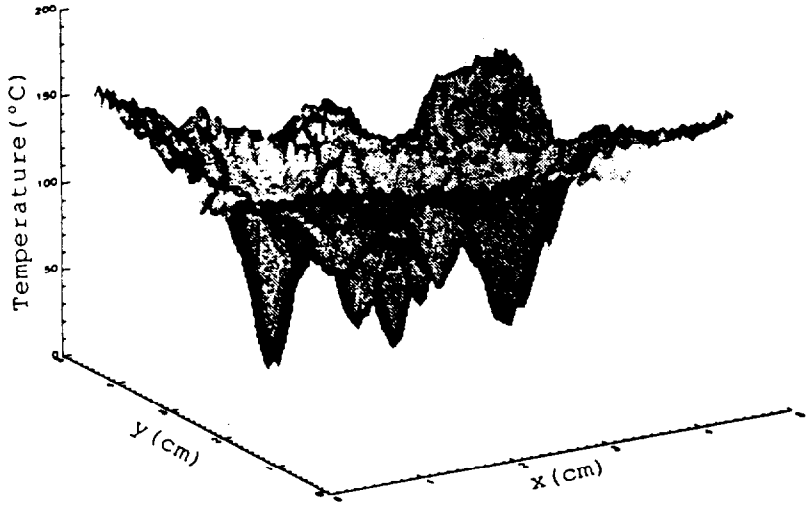

Figure 27 - Surface Plots: T_o = 182°C, G = 1.3 g/m²s

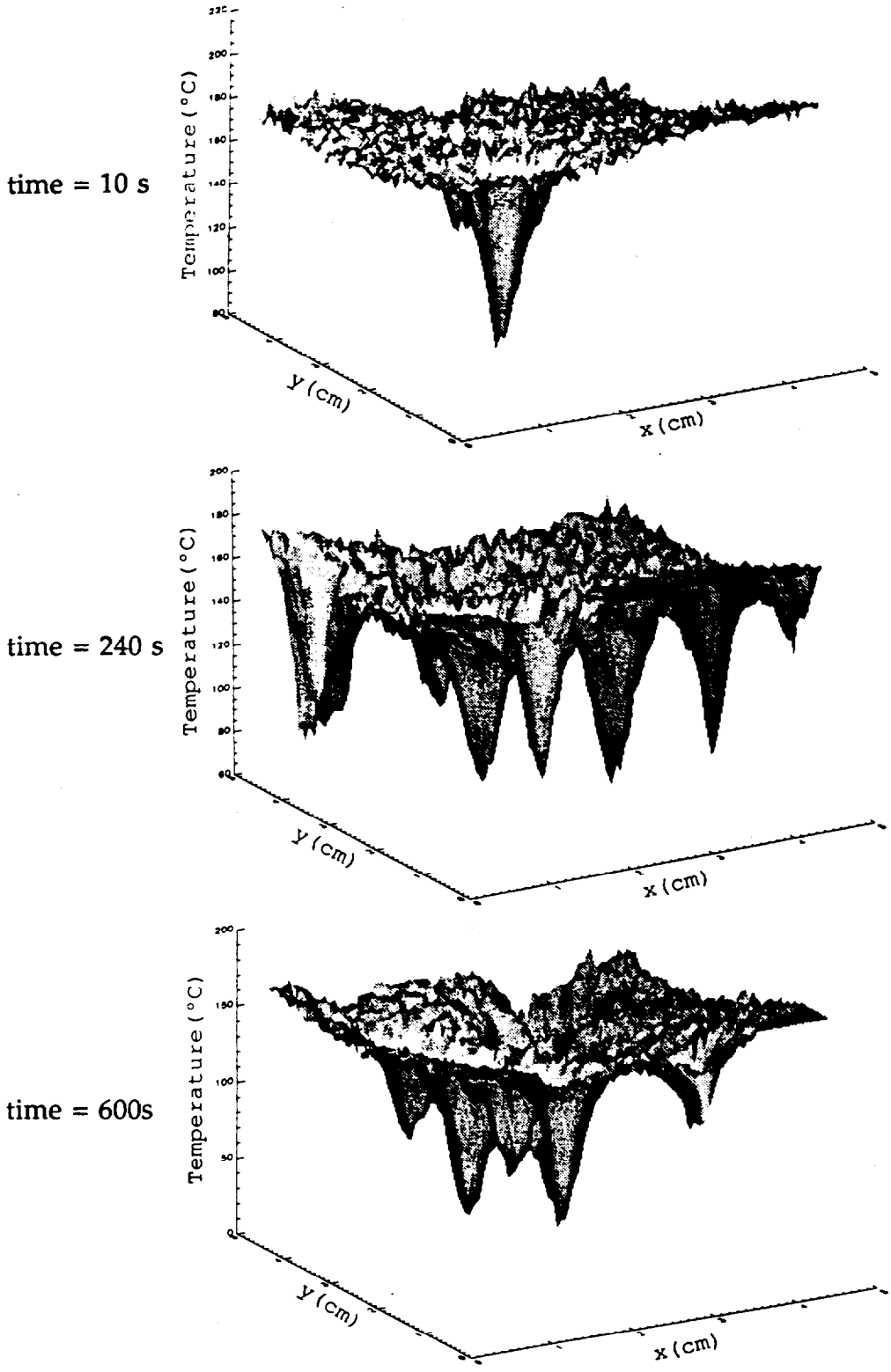

Figure 28 - Surface Plots: T_o = 182°C, G = .86 g/m²s

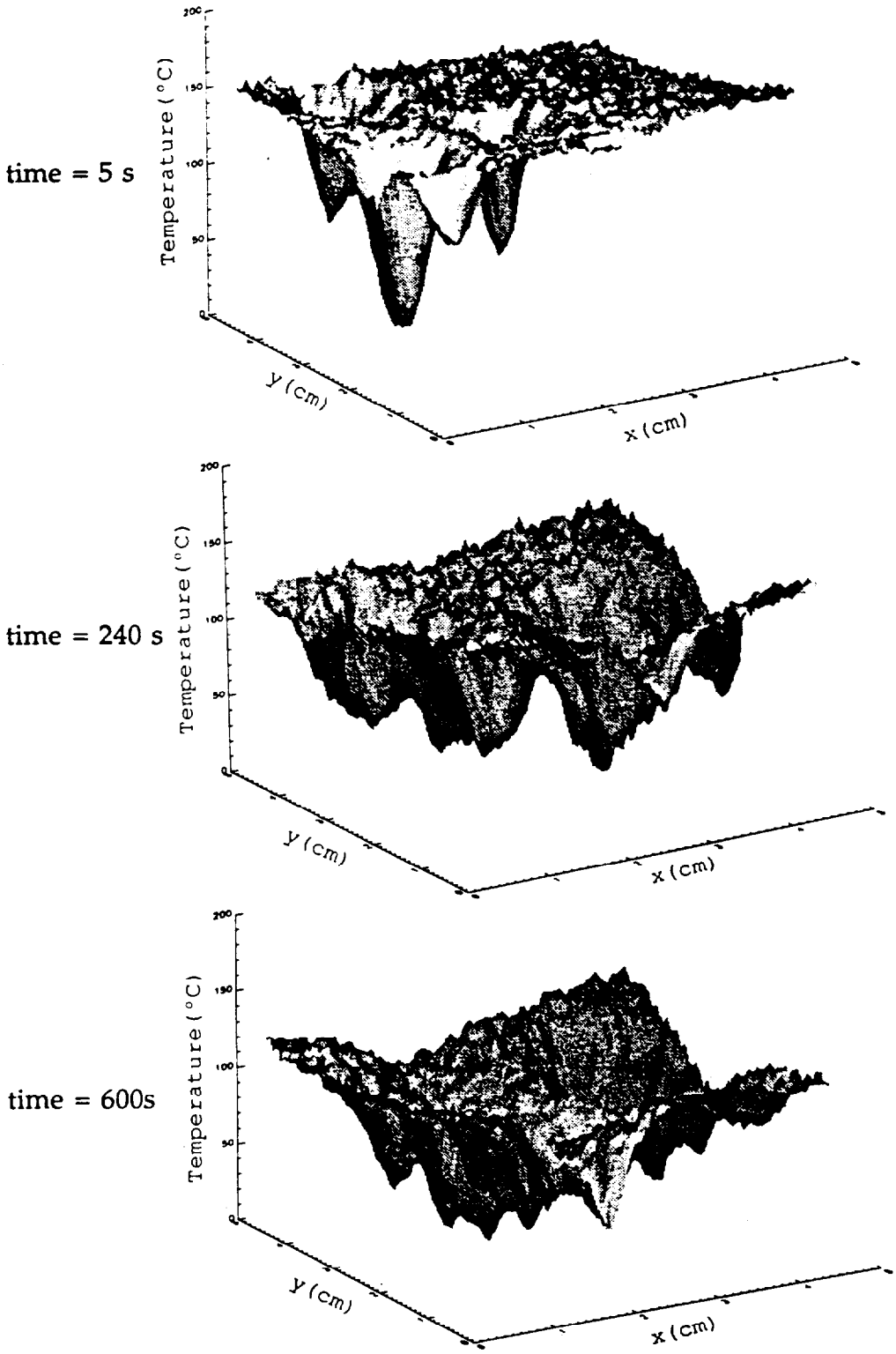

Figure 29 - Surface Plots: T_o = 162°C, G = 1.5 g/m^{2}s

time = 10 s

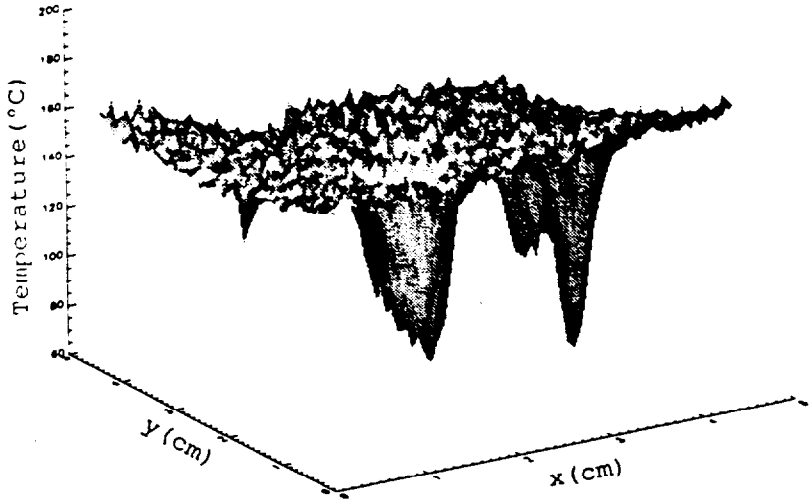

time = 240 s

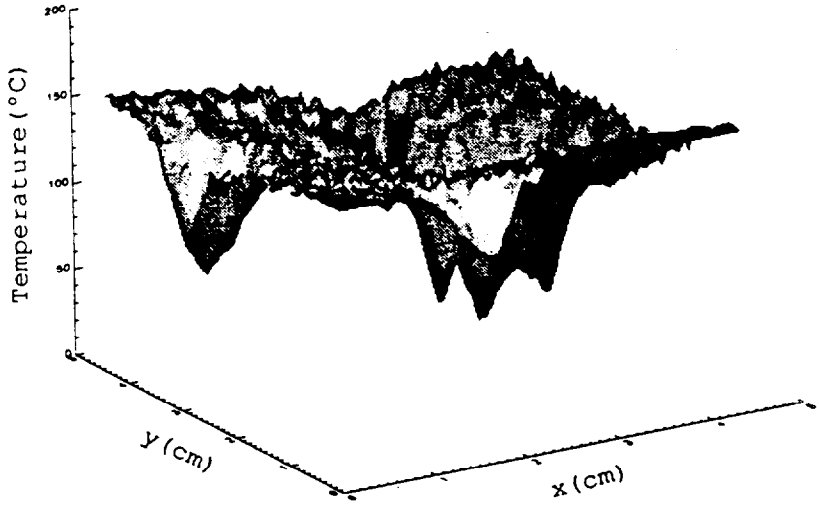

time = 600s

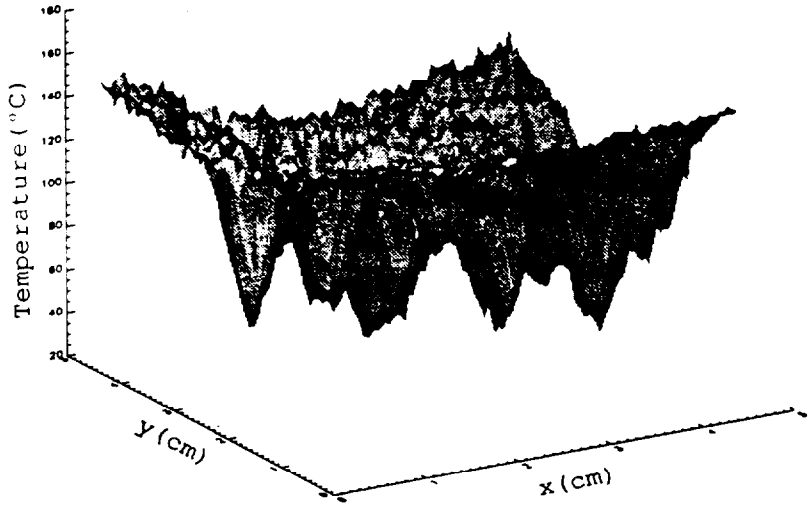

Figure 30 - Surface Plots: T_o = 162°C, G = .97 g/m^{2}s

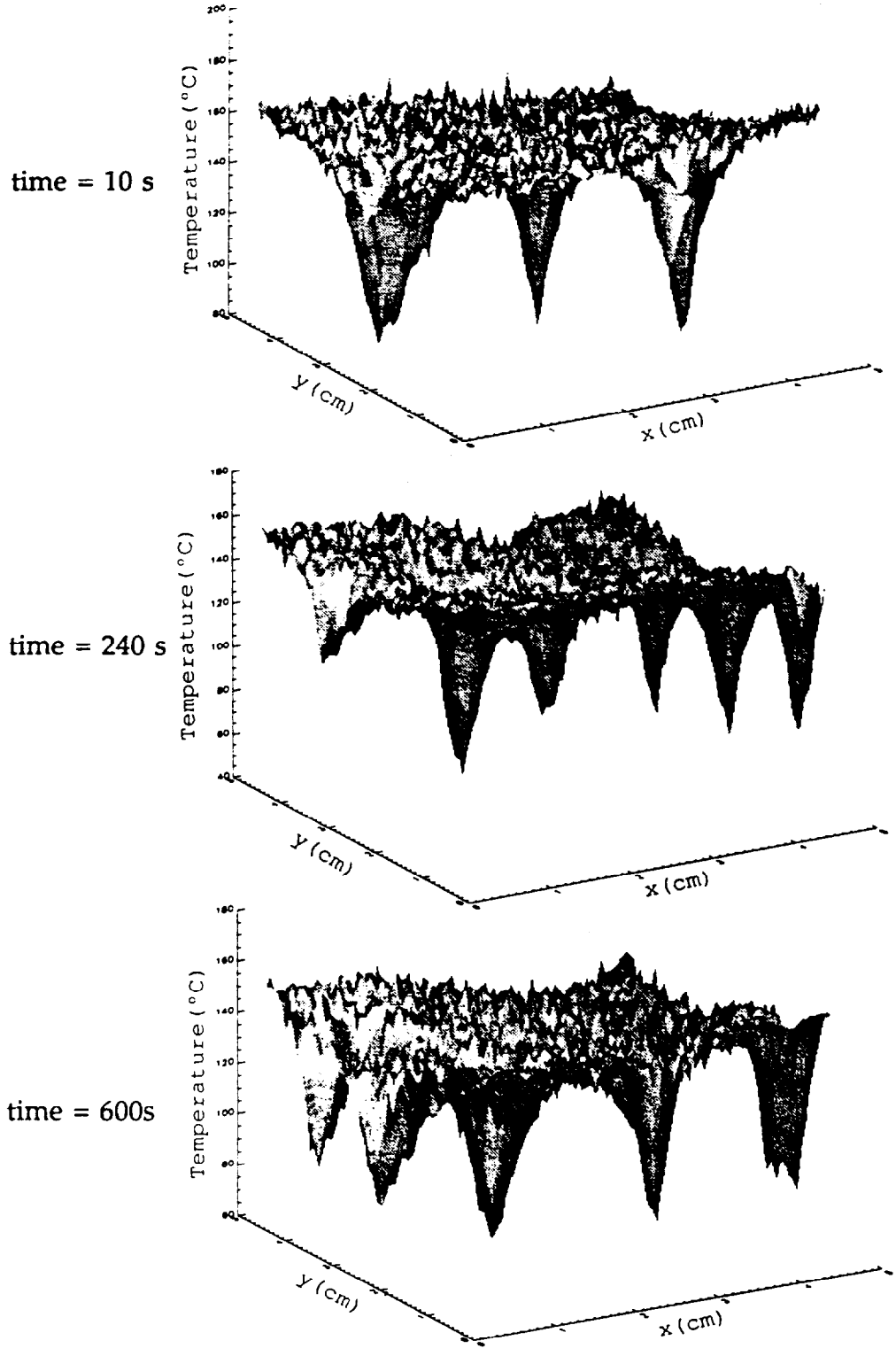

Figure 31 - Surface Plots: T_o = 162°C, G = .51 g/m^{2}s

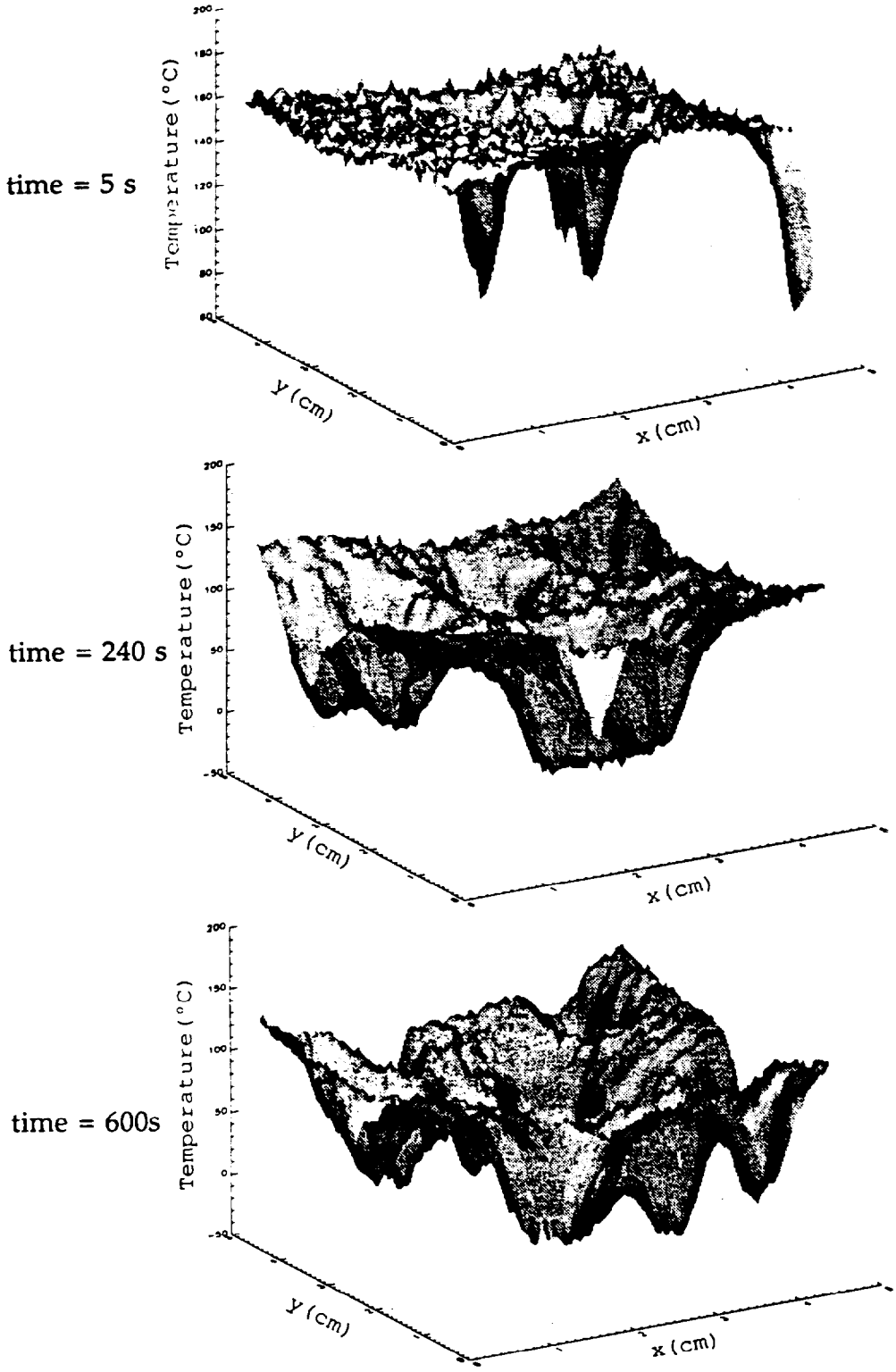

Figure 32 - Surface Plots: T_o = 151°C, G = 1.8 g/m^{2}s

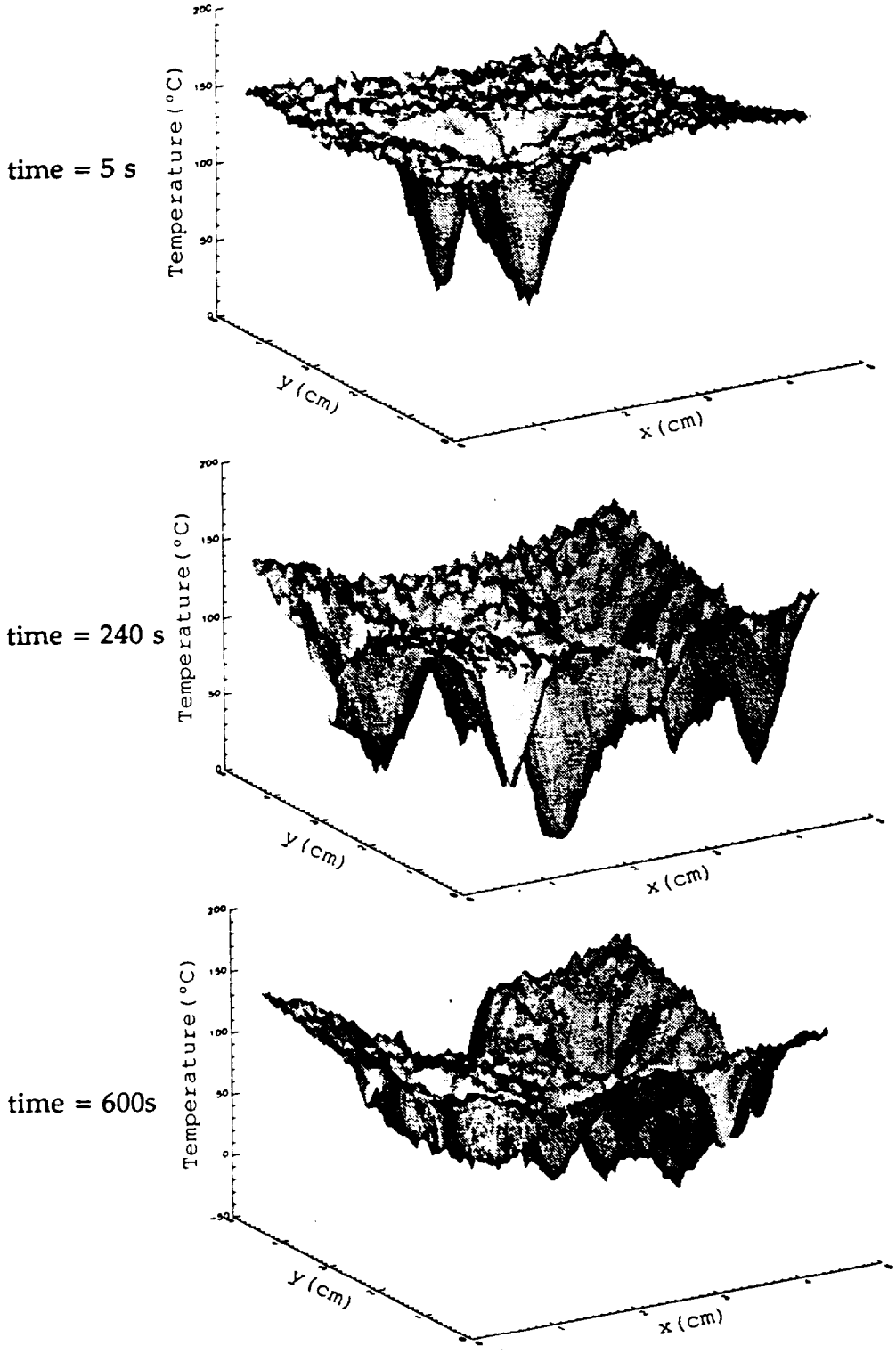

Figure 33 - Surface Plots: T_o = 151°C, G = 1.3 g/m^{2}s

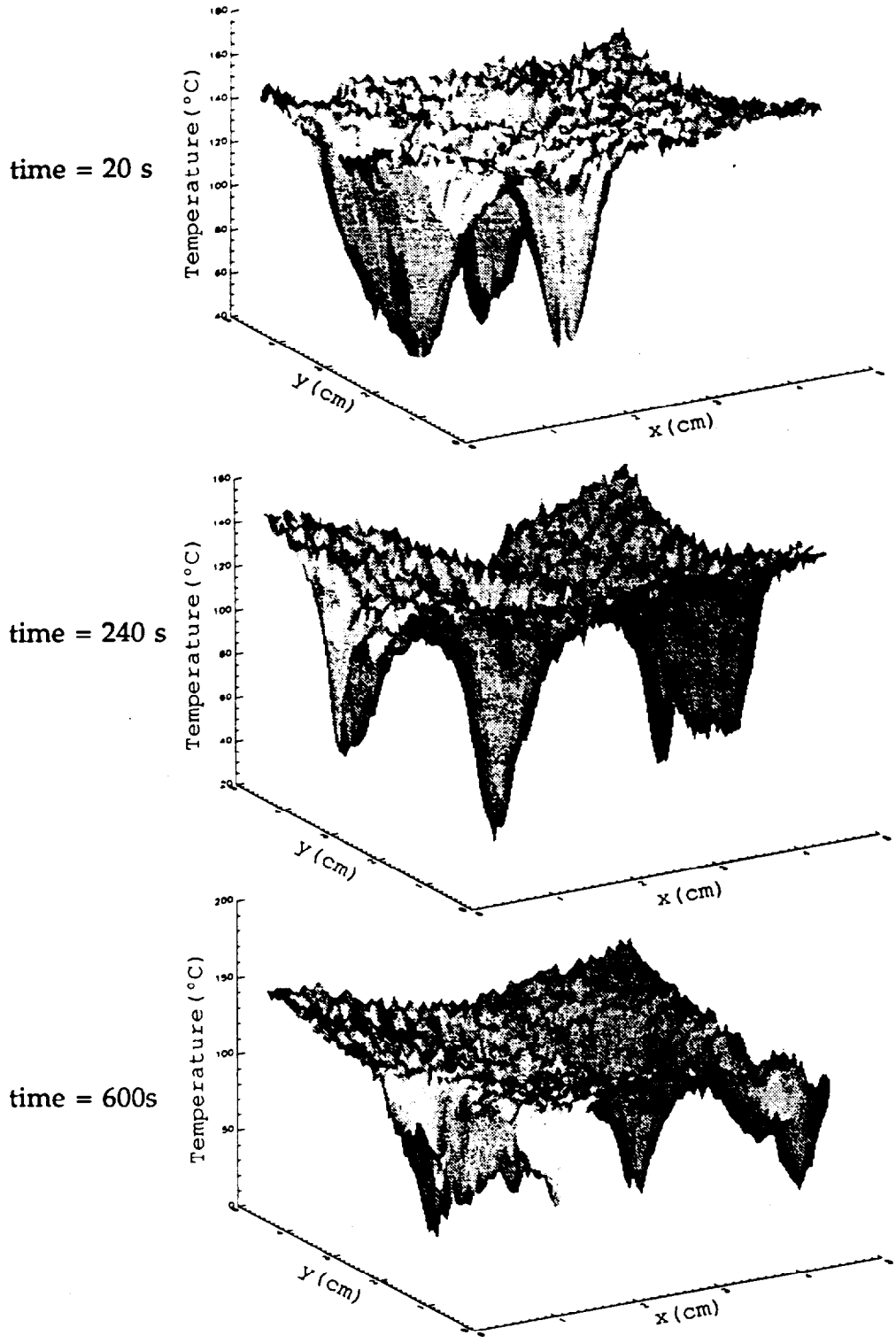

Figure 34 - Surface Plots: T_o = 151°C, G = .96 g/m^{2}s

time = 20 s

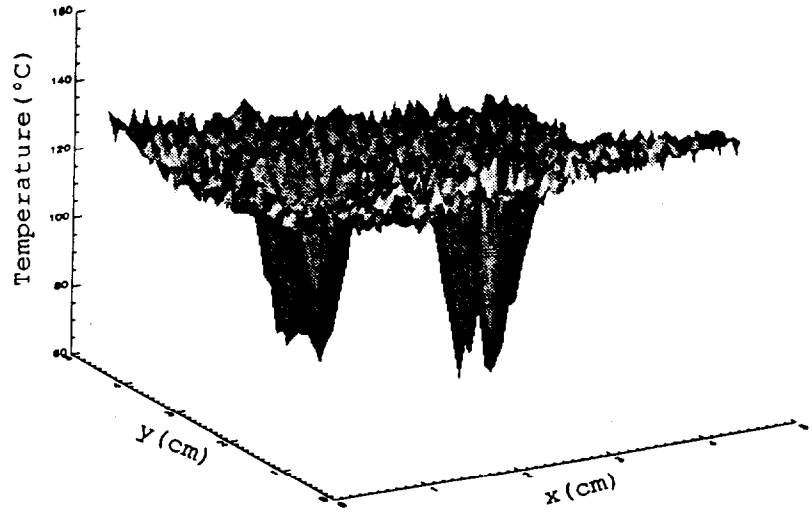

time = 240 s

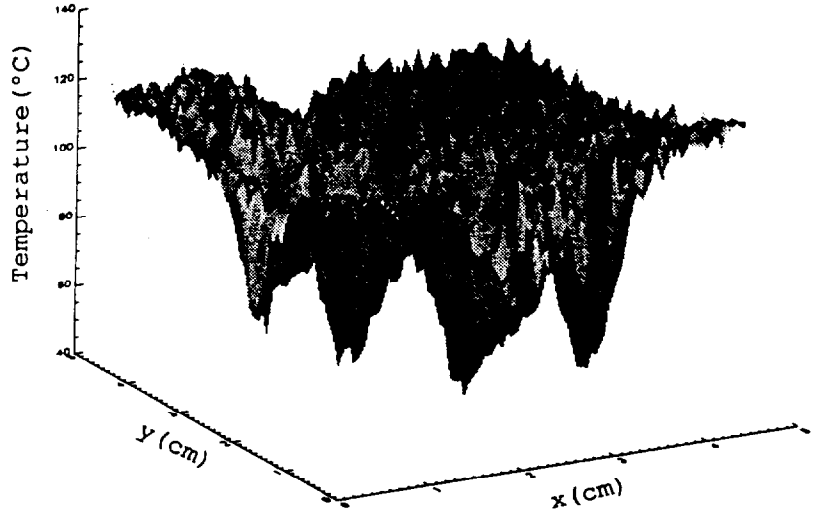

time = 600s

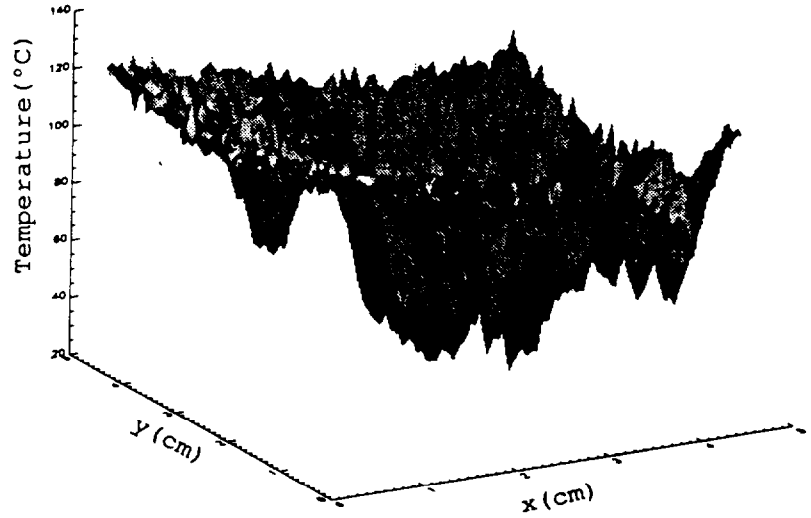

Figure 35 - Surface Plots: T_o = 131°C, G = .67 g/m^{2}s

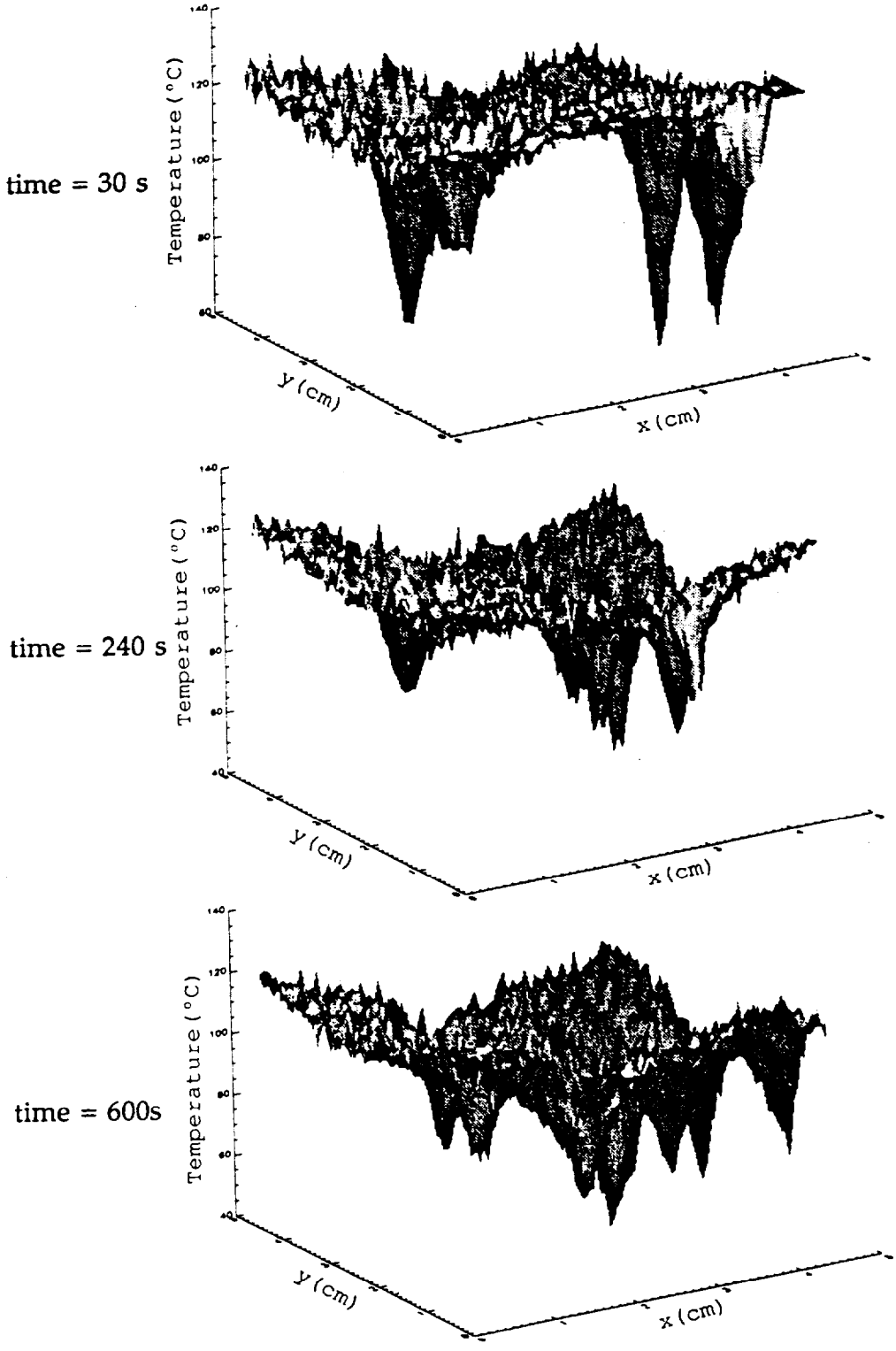

Figure 36 - Surface Plots: T_o = 131°C, G = .5 g/m²s

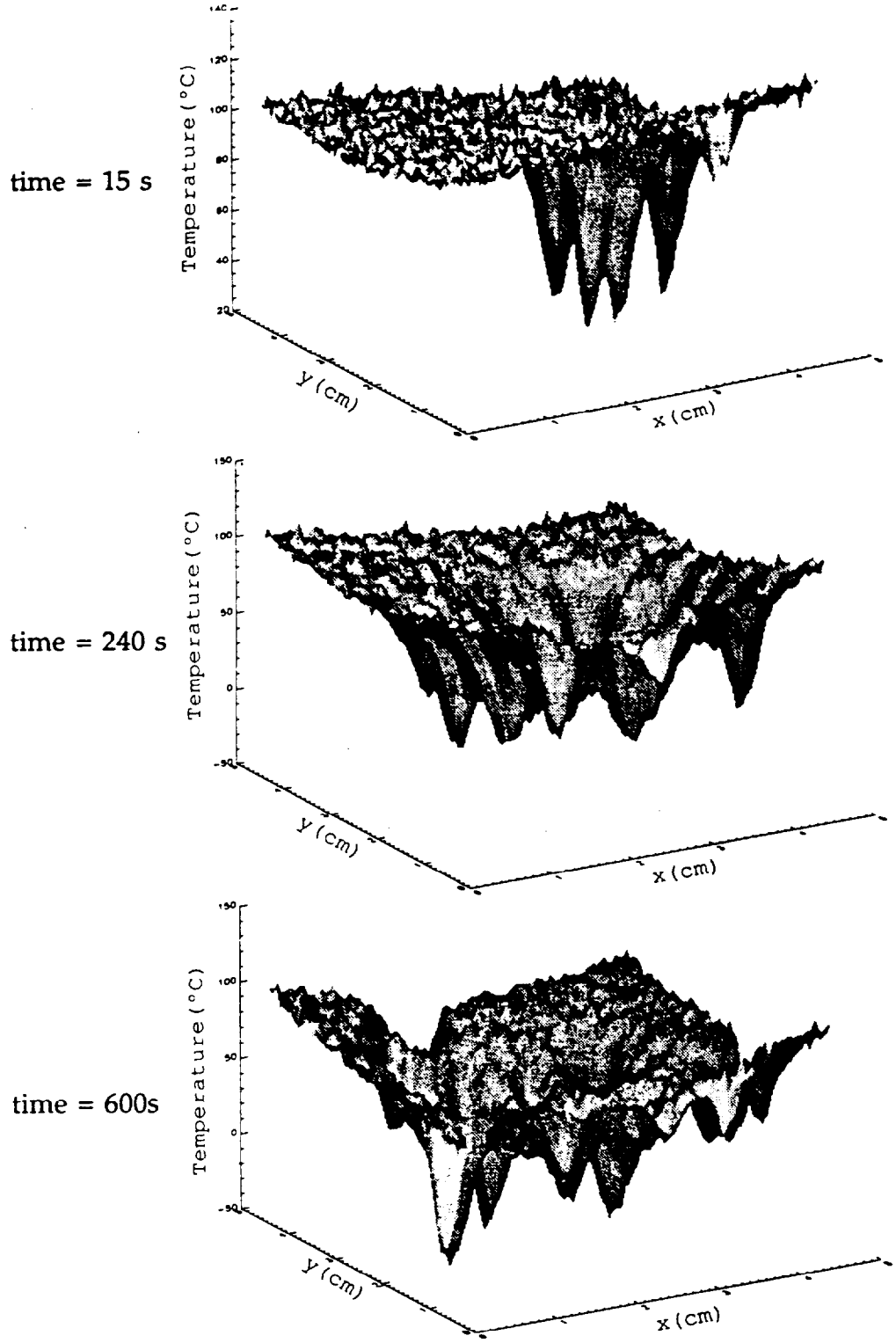

Figure 37 - Surface Plots: T_o = 111°C, G = .54 g/m^{2}s

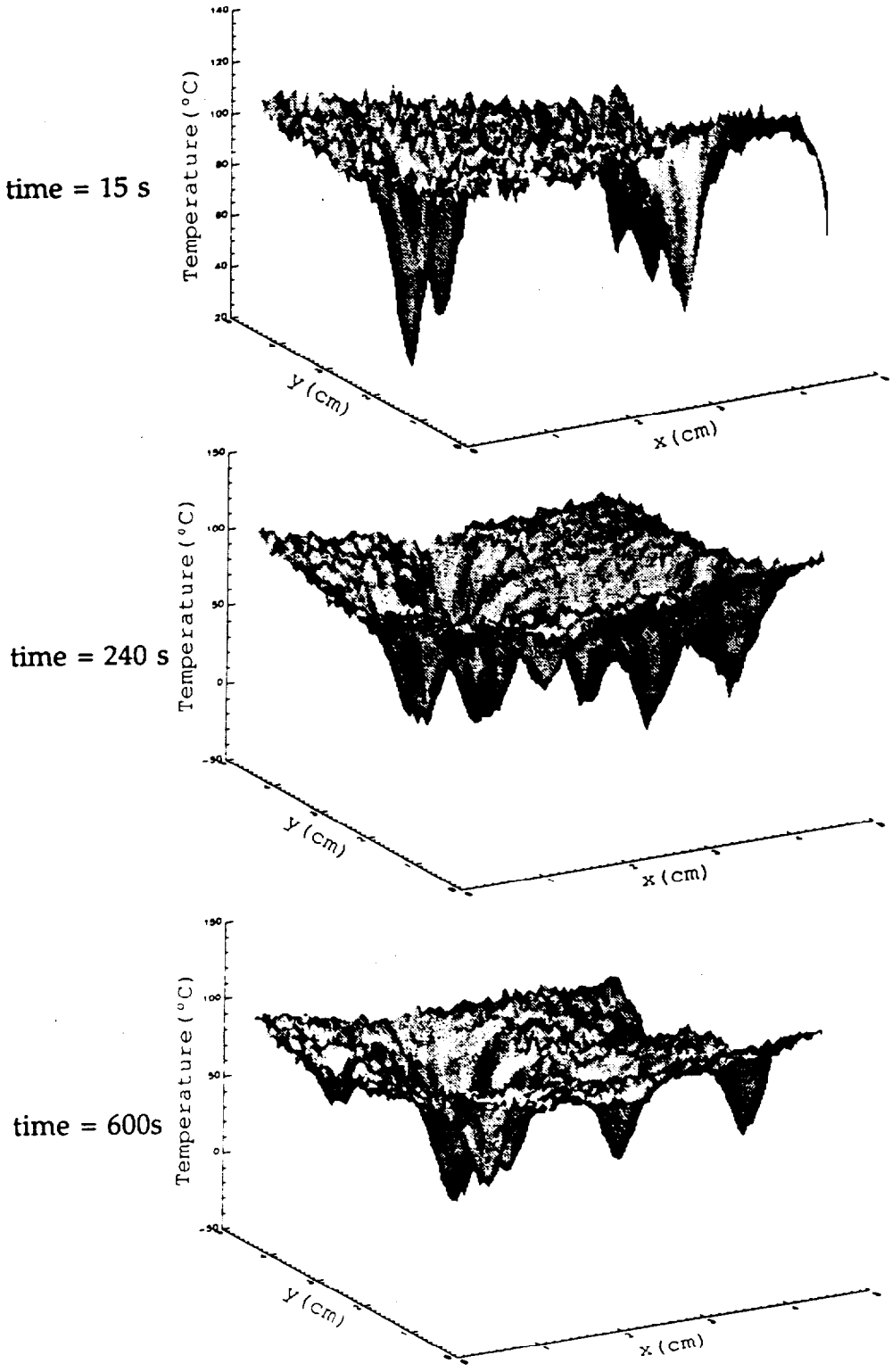

Figure 38 - Surface Plots: T_o = 111°C, G = .36 g/m^{2}s

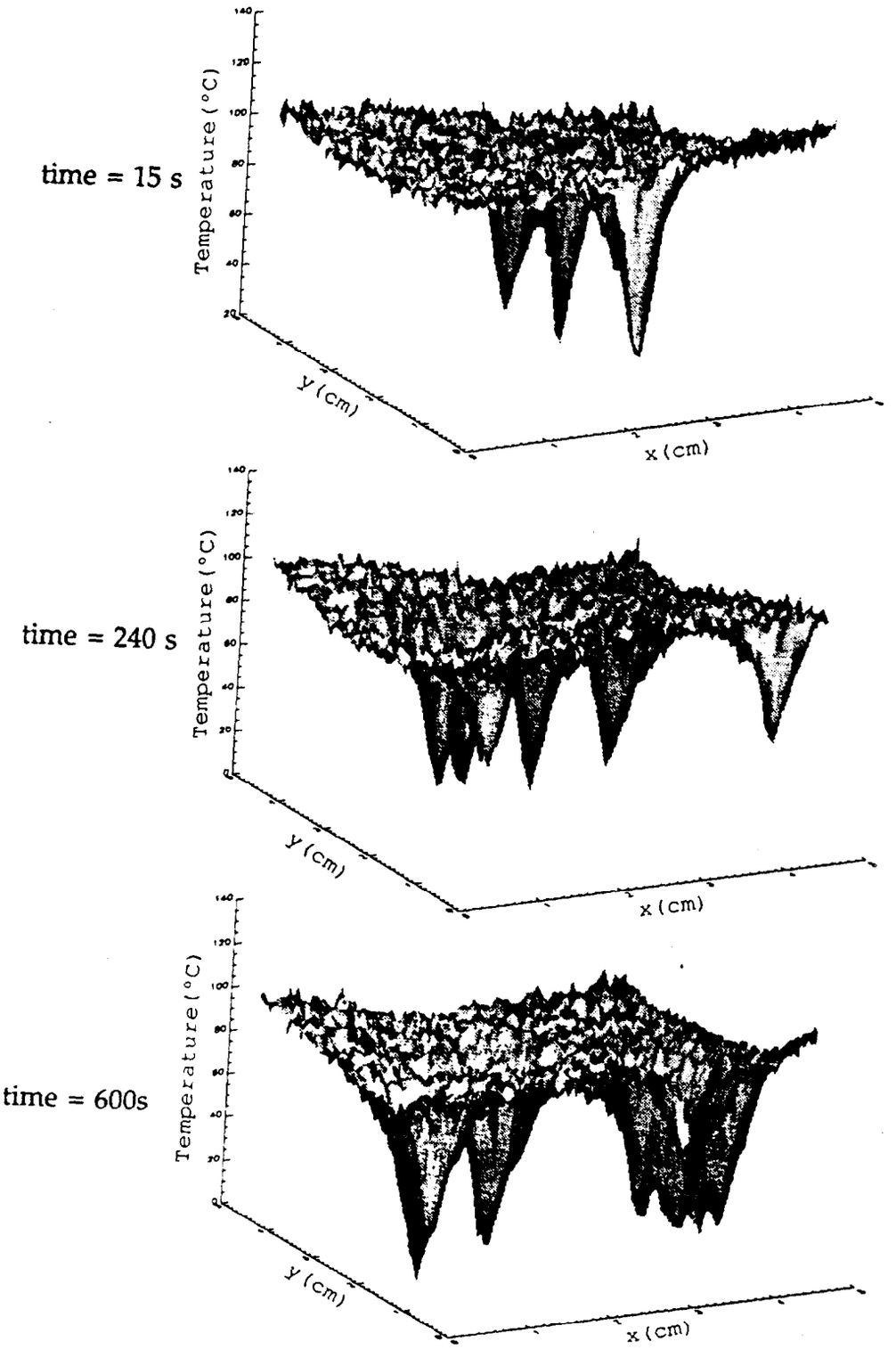

Figure 39 - Surface Plots: T_o = 111°C, G = .24 g/m^{2}s

APPENDIX B - RAW DATA

Time (min.)	G=.0016 kg/m²s	G=.0013 kg/m²s	G=.00086 kg/m²s
0	182	182	182
.5	157.69	160.0	173.69
1.0	146.49	152.02	165.99
1.5	142.32	148.16	166.54
2.0	131.10	139.47	162.53
2.5	126.87	133.04	163.18
3.0	123.98	133.62	161.25
3.5	123.47	126.27	160.55
4.0	119.93	124.22	160.17
4.5	115.41	124.89	159.14
5.0	117.76	123.47	157.17
5.5	117.49	129.26	156.65
6.0	112.98	127.42	154.12
6.5	114.34	125.99	155.57
7.0	113.9	126.78	153.82
7.5	111.28	128.17	153.53
8.0	109.33	123.02	149.11
8.5	111.07	120.7	152.23
9.0	107.48	122.68	153.92
9.5	111.25	121.04	151.03
10.0	109.08	122.62	149.97
10.5	105.61	119.37	149.92
11.0	100.46	121.79	149.61
11.5	104.77	122.65	151.60

Table 2 - Temperature vs. Time for Various Mass Fluxes

12.0	105.69	116.74	148.37
12.5	104.78	122.43	147.51
13.0	105.24	118.406	149.21
13.5	104.78	119.401	151.31
14.0	105.06	117.406	148.62
14.5	103.52	118.1	149.69
15.0	106.48	119.48	149.94
15.5	104.56	122.75	148.80
16.0	104.06	117.73	153.20
16.5	106.93	123.21	151.01
17.0	103.79	121.25	152.01
17.5	103.89	121.18	148.24
18.0	102.36	123.01	148.36
18.5	99.84	123.27	149.72
19.0	98.99	121.83	149.50
19.5	107.14	122.91	151.37
20.0	106.06	119.48	152.67
20.5	101.5	119.62	150.14
21.0	104.16	121.24	153.01
21.5	106.28	117.9	151.36
22.0	105.94	115.42	150.48
22.5	100.29	118.37	148.10
23.0	103.0	117.78	147.90
23.5	98.61	115.23	148.4
24.0	103.18	113.01	152.59

Table 2 continued

Time (min.)	G=.0015 kg/m^{2}s	G=.00097 kg/m^{2}s	G=.00051 kg/m^{2}s
0	162	162	162
.5	144.79	153.74	147.09
1.0	130.30	148.92	140.63
1.5	119.73	143.44	141.08
2.0	117.91	140.18	137.91
2.5	113.21	139.07	135.87
3.0	115.75	133.52	135.30
3.5	109.85	137.56	134.46
4.0	111.48	136.15	137.02
4.5	105.02	134.22	135.87
5.0	99.12	127.32	137.70
5.5	94.34	132.99	136.05
6.0	92.63	126.38	132.70
6.5	94.65	125.85	132.84
7.0	97.49	124.64	130.62
7.5	93.06	125.19	130.01
8.0	93.23	124.86	128.51
8.5	91.90	125.0	130.15
9.0	90.33	120.65	126.07
9.5	90.36	122.04	127.75
10.0	92.88	122.56	128.26
10.5	85.71	122.57	130.10
11.0	83.74	120.33	127.86
11.5	82.74	122.63	126.68

Table 3 - Temperature vs. Time for Various Mass Fluxes

12.0	84.45	120.84	129.62
12.5	85.0	120.01	130.94
13.0	87.36	118.6	132.35
13.5	82.89	122.72	132.46
14.0	74.12	123.84	131.13
14.5	75.34	124.19	130.58
15.0	74.15	121.72	128.82
15.5	80.40	120.36	130.41
16.0	85.57	122.58	131.99
16.5	83.39	125.46	129.50
17.0	80.67	122.43	132.26
17.5	76.29	118.63	131.34
18.0	76.87	120.55	131.60
18.5	78.33	121.83	130.10
19.0	77.09	120.44	128.77
19.5	77.36	120.83	128.41
20.0	69.14	124.01	126.87
20.5	70.27	121.76	130.77
21.0	70.39	118.57	132.77
21.5	72.74	117.10	131.60
22.0	73.74	120.42	130.00
22.5	74.15	122.58	131.67
23.0	77.83	120.71	129.09
23.5	74.04	120.99	128.80
24.0	69.68	119.4	128.51

Table 3 continued

Time (min.)	G=.0018 kg/m²s	G=.0013 kg/m²s	G=.00096 kg/m²s
0	151	151	151
.5	138.16	130.13	139.00
1.0	119.72	122.12	131.62
1.5	119.55	116.88	129.64
2.0	114.57	114.85	126.57
2.5	110.26	108.65	125.62
3.0	105.74	110.21	125.41
3.5	98.97	108.85	118.60
4.0	99.80	102.13	122.42
4.5	93.19	104.64	118.45
5.0	96.16	104.68	119.79
5.5	95.41	99.04	110.91
6.0	92.28	95.06	109.05
6.5	98.54	97.77	113.08
7.0	95.23	97.19	115.05
7.5	90.31	97.54	113.57
8.0	84.41	96.99	115.52
8.5	90.84	92.05	113.24
9.0	84.71	94.48	116.71
9.5	83.57	93.87	112.66
10.0	83.28	91.28	113.65
10.5	84.09	90.32	109.04
11.0	83.30	91.29	111.42
11.5	80.92	90.98	110.45

Table 4 - Temperature vs. Time for Various Mass Fluxes, T_o=151°C

12.0	82.35	90.45	110.71
12.5	78.90	88.34	110.97
13.0	80.20	92.33	109.86
13.5	84.70	91.17	112.78
14.0	80.15	93.12	108.06
14.5	82.73	92.29	108.34
15.0	76.15	89.59	108.3
15.5	75.21	86.49	
16.0	76.55	88.48	
16.5	76.87	89.34	
17.0	76.96	89.82	
17.5	78.70	91.72	
18.0	75.06	91.84	
18.5	76.30	91.87	
19.0	71.98	93.65	
19.5	72.14	92.75	
20.0	73.23	91.14	
20.5	77.48	90.21	
21.0	68.86	88.85	
21.5	71.88	86.53	
22.0	74.70	87.55	
22.5	72.61	89.45	
23.0	72.95	86.24	
23.5	74.44	91.32	
24.0	74.13	94.68	

Table 4 continued

Time (min.)	G=.00067 kg/m²s	G=.0005 kg/m²s	G=.00082 kg/m²s
0	131	131	131
.5	121.28	125.91	120.8
1.0	114.19	122.85	116.24
1.5	112.31	117.90	112.10
2.0	110.04	114.70	110.68
2.5	108.49	112.90	109.19
3.0	109.80	108.99	105.43
3.5	109.71	108.39	105.89
4.0	110.36	109.3	106.26
4.5	109.42	108.92	102.04
5.0	105.73	109.01	100.36
5.5	108.18	106.37	99.79
6.0	107.14	106.52	98.81
6.5	106.65	106.22	96.72
7.0	103.61	104.84	96.39
7.5	103.28	105.12	95.87
8.0	101.12	104.11	93.44
8.5	98.78	103.22	91.74
9.0	95.78	104.36	90.28
9.5	94.08	103.28	87.22
10.0	96.20	102.73	85.28
10.5	94.57	102.55	87.60
11.0	93.69	103.63	86.16
11.5	93.64	101.42	86.42

Table 5 - Temperature vs. Time for Various Mass Fluxes, T_o=131°C

12.0	93.45	101.48	84.72
12.5	95.17	101.23	82.78
13.0	97.96	100.45	83.76
13.5	97.06	100.21	82.9
14.0	94.94	98.04	82.17
14.5	93.55	97.23	80.90
15.0	92.18	99.29	77.95
15.5	89.92	100.53	76.90
16.0	89.89	101.74	75.57
16.5	89.84	99.85	74.58
17.0	89.15	100.69	74.03
17.5	88.05	101.79	72.57
18.0	90.03	100.87	68.69
18.5	92.37	101.82	68.55
19.0	93.63	101.19	70.22
19.5	95.37	101.41	69.15
20.0	93.22	100.17	69.70
20.5	91.08	101.65	69.93
21.0	93.38	100.58	69.34
21.5	93.26	102.20	69.02
22.0	92.44	101.85	68.07
22.5	90.83	102.83	66.64
23.0	91.37	101.95	68.31
23.5	91.03	102.95	70.97
24.0	89.91	102.39	69.89

Table 5 continued

Time (min.)	G=.00054 kg/m^{2}s	G=.0036 kg/m^{2}s	G=.00024 kg/m^{2}s
0	111	111	111
.5	100.11	104.76	105.43
1.0	91.68	99.33	100.02
1.5	85.16	94.41	98.77
2.0	80.72	87.58	96.43
2.5	79.50	86.33	97.90
3.0	72.48	86.09	98.56
3.5	73.23	84.18	96.68
4.0	69.92	82.12	93.87
4.5	68.86	80.04	95.01
5.0	70.80	79.80	91.26
5.5	68.88	81.17	89.56
6.0	65.32	83.76	92.22
6.5	65.82	80.27	91.97
7.0	66.83	79.81	92.51
7.5	63.30	80.20	92.46
8.0	60.81	79.33	92.77
8.5	58.82	80.15	91.74
9.0	63.60	80.25	89.63
9.5	57.96	77.38	87.36
10.0	56.93	79.65	85.69
10.5	62.16	79.63	89.57
11.0	62.85	78.69	88.08
11.5	58.89	74.90	85.60

Table 6 - Temperature vs. Time for Various Mass Fluxes, T_o=111°C

12.0	63.09	76.41	81.10
12.5	63.73	78.96	83.43
13.0	62.82	76.88	80.68
13.5	61.93	78.78	82.10
14.0	59.32	76.88	81.22
14.5	55.70	80.31	84.37
15.0	56.57	76.55	83.60
15.5	60.65	76.21	80.65
16.0	59.59	75.34	80.69
16.5	61.81	77.51	81.71
17.0	57.94	76.91	81.57
17.5	57.47	76.58	83.94
18.0	59.66	75.28	81.64
18.5	60.21	73.14	80.86
19.0	60.67	75.28	83.54
19.5	60.53	75.02	81.79
20.0	59.24	73.94	80.53
20.5	57.80	76.74	79.90
21.0	60.14	75.16	79.27
21.5	63.82	76.47	80.24
22.0	60.69	74.96	83.06
22.5	60.54	73.24	84.50
23.0	59.32	75.00	82.68
23.5	60.60	76.89	83.52
24.0	60.18	76.44	79.63

Table 6 continued

APPENDIX C - COMPUTER CODE

```
/* PIXAV.C – Averages the pixel intensities over a selected portion of a
frame*/

/* Include necessary C libraries*/

#include <stdio.h>
#include <stdlib.h>
#include <limits.h>
#include <float.h>
#include <string.h>

main(int argc, char *argv[])
{

/* Declaration of variables and parameters*/
int sbuf,value,backbuf,winbuf,overlaybuf,source,model,display,chan,fbuf,
mode2;
int dbuf,x,y,membase,iobase,mode,count,fcount;
unsigned long im_pixr(x,y),pixel;
float av,temp,templ,total;
FILE *fp;

/* Declaration of Imager-AT library functions*/
int im_init(membase,iobase),im_snapshot(dbuf);
int im_inmode(mode),im_opmode(mode2,fbuf),
   im_clear(sbuf,value);
void im_video(display,source),im_sync(source,chan),
    im_outpath(bachbuf,winbuf,overlaybuf,source),
    im_procwin(x1,y1,x2,y2),im_gain(value),
    im_offset(value),im_outmode(mode);

/* Initialize MVP-AT board, clear frame buffer, set up frame display, set
up operating mode for processing */
       im_init(0xd00,0x300);
       im_clear(0,0);
       im_outpath(0,-1,0,0);
       im_inmode(1);
       im_video(1,1);
       im_sync(1,0);
       im_opmode(2,0);


/* Set offset and gain values on grabber board */
       im_offset(0);
```

```
        im_gain(0);

/* Allow electronics to sync up, graba frame, set operating mode for
  I/O*/
        im_snapshot(0);
        im_clear(0,0);
        im_snapshot(0,0);
        im_clear(0,0);
        im_snapshot(0);
        im_clear(0,0);
        im_snapshot(0);
        im_opmode(0,0);
        im_outmode(0);

        total= 0.;
        count = 0;
        fcount = 1;

/* Read and total pixel intensity values over the defined region, and feed
to a file */
        if (argc !=2)
        {
           printf("Usage: %s filename(for
             output)\n",argv[0]);
           exit(1);
        }
        fp = fopen(argv[1],"w");

        for (x=84;x<=398;x+=5)
        {
         for (y=108;y<=401:y+=5)
         {
         pixel = im_pixr(x,y);
             total = total + pixel;
             templ = (1.165*(float)pixel- 17.54;
         count++;
             printf("%d %d %f\n",x,y,templ);
             if (fcount <= 29)
         {

           fprintf(fp,"%.2f",templ);
              fcount++;
         }
         else
```

```
                {
                fprintf(fp,"%.2f \n",templ);
                fcount = 1;
              }
            }
           }
 /* Compute average pixel intensity and print values for total and
    averages */
          av = total/(float)count;
          temp =(1.165*av) - 17.54
          printf("total pixels read = %d\n",count);
          printf("sum of pixels = %f\n",total);
          printf("pixel average (decimal) = %f\n",av);
          printf("temperature = %f deg C\n",temp);

         if (fclose(fp) !=0)
        printf("error closing file\n");
         else
           printf("File %s successfully closed\n", argv[1])
     return(0);
}
```

REFERENCES

1. W.M. Grissom and F.A. Wierum, "Liquid Spray Cooling of a Heated Surface", International Journal of Heat and Mass Transfer, Vol. 24, pp. 261-271, 1981.

2. L.L. Levitan and F.P. Lantsman, "Investigating Burnout with Flow of a Steam-Water Mixture in a Round Tube", Thermal Engineering, 22, p. 102, 1975.

3. I.C. Finlay, "Spray Flow as a Heat Transfer Media", Chem. Process., 5, pp. 25-29, 1971.

4. M.M. Fikry, "Heat Transfer to Wet Steam Flowing in a Horizontal Tube", Ph.D. Thesis, University of London, 1952.

5. P. Savic and G.T. Boult, "The Fluid Flow Associated with the Impact of Liquid Drops with Solid Surfaces", National Research Council of Canada, Report No. mt-26, 1955.

6. M. Klassen, M. diMarzo, J. Sirkis, "Infrared Thermography of Dropwise Evaporative Cooling", ASME HTD, Vol. 141, pp. 117-121, 1990.

7. C. Kidder, "Dropwise Evaporative Cooling of a Ceramic Solid Surface Heated by Radiation", Master of Science, University of Maryland at College Park, 1990.

8. M. diMarzo, C.H. Kidder, P. Tartarini, "Infrared Thermography of Dropwise Evaporative Cooling of a Semi-Infinite Solid Subjected to Radiant Heat Input", Experimental Heat Transfer, Vol. 5, pp. 101-104, 1992.

9. Abu-Zaid and Atreya, "Effect of Water on Piloted Ignition of Celluosic Materials", NIST, Interagency Report, NIST-GCR-89-561, 1989.

10. M. Seki, H. Kawamura, K. Sanokawa, "Transient Temperature Profile of a Hot Wall Due to an Impinging Liquid Droplet", Journal of Heat Transfer, Vol. 100, p. 167, 1978.

11. C. Bonacina, S. Del Guidice, G. Comini, "Dropwise Evaporation", ASME Journal of Heat Transfer, Vol. 101, pp. 441-446, 1979.

12. K. Makino, I. Michiyoshi, "The Behavior of a Water Droplet on a Heated Surfaces", International Journal of Heat and Mass Transfer, Vol. 27, pp. 781-791, 1984.

13. Y. Liao, "Dropwise Evaporative Cooling of Solid Surfaces", Doctoral Dissertation, University of Maryland, 1992.

14. R.A. Lavash, "Water Droplet Dispenser Control", Class Project Report, University of Maryland, 1990.

15. C.T. Avedisian, S. Chandra, "On the Collision of a Droplet with a Solid Surface", Proceedings of the Royal Society of London, Vol. 432, pp. 13-41, 1991.

NIST-114
(REV. 9-92)
ADMAN 4.09

U.S. DEPARTMENT OF COMMERCE
NATIONAL INSTITUTE OF STANDARDS AND TECHNOLOGY

MANUSCRIPT REVIEW AND APPROVAL

(ERB USE ONLY)
ERB CONTROL NUMBER | DIVISION
PUBLICATION REPORT NUMBER: NIST-GCR-93-624 | CATEGORY CODE
PUBLICATION DATE: April 1993 | NUMBER PRINTED PAGE

INSTRUCTIONS: ATTACH ORIGINAL OF THIS FORM TO ONE (1) COPY OF MANUSCRIPT AND SEND TO: THE SECRETARY, APPROPRIATE EDITORIAL REVIEW BOARD.

TITLE AND SUBTITLE (CITE IN FULL)

AN EXPERIMENTAL STUDY OF MULTIPLE DROPLET EVAPORATIVE COOLING

CONTRACT OR GRANT NUMBER: GRANT NO. 70NANB1H1173

TYPE OF REPORT AND/OR PERIOD COVERED: Final Report, December 1992

AUTHOR(S) (LAST NAME, FIRST INITIAL, SECOND INITIAL)

H. Dawson, M. di Marzo
University of Maryland
Mechanical Engineering Department
College Park, MD 20742

PERFORMING ORGANIZATION (CHECK (X) ONE BOX)
[ ] NIST/GAITHERSBURG
[ ] NIST/BOULDER
[ ] JILA/BOULDER

LABORATORY AND DIVISION NAMES (FIRST NIST AUTHOR ONLY)

SPONSORING ORGANIZATION NAME AND COMPLETE ADDRESS (STREET, CITY, STATE, ZIP)

U.S. Department of Commerce
National Institute of Standards and Technology
Gaithersburg, MD 20899

RECOMMENDED FOR NIST PUBLICATION

[ ] JOURNAL OF RESEARCH (NIST JRES)
[ ] J. PHYS. & CHEM. REF. DATA (JPCRD)
[ ] HANDBOOK (NIST HB)
[ ] SPECIAL PUBLICATION (NIST SP)
[ ] TECHNICAL NOTE (NIST TN)
[ ] MONOGRAPH (NIST MN)
[ ] NATL. STD. REF. DATA SERIES (NIST NSRDS)
[ ] FEDERAL INF. PROCESS. STDS. (NIST FIPS)
[ ] LIST OF PUBLICATIONS (NIST LP)
[ ] NIST INTERAGENCY/INTERNAL REPORT (NISTIR)
[ ] LETTER CIRCULAR
[ ] BUILDING SCIENCE SERIES
[ ] PRODUCT STANDARDS
[X] OTHER NIST-GCR

RECOMMENDED FOR NON-NIST PUBLICATION (CITE FULLY) [ ] U.S. [ ] FOREIGN

PUBLISHING MEDIUM
[X] PAPER [ ] CD-RO
[ ] DISKETTE (SPECIFY)
[ ] OTHER (SPECIFY)

SUPPLEMENTARY NOTES

ABSTRACT (A 1500-CHARACTER OR LESS FACTUAL SUMMARY OF MOST SIGNIFICANT INFORMATION. IF DOCUMENT INCLUDES A SIGNIFICANT BIBLIOGRAPHY OR LITERATURE SURVEY, CITE IT HERE. SPELL OUT ACRONYMS ON FIRST REFERENCE.) (CONTINUE ON SEPARATE PAGE, IF NECESSARY.)

Techniques of infrared thermography were used to conduct an experimental study of the evaporative cooling of a hot, low thermal conductivity, non-metallic surface heated by radiation and subject to a random array of impinging water droplets. A droplet generating ar distributing apparatus and a data acquisition system employing digital image analysis device were also developed and implemented. Real time infrared images of the heated surface were recorded and digitized using computer resident fram grabbing hardware and analyzed on a pizel bases, giving a high degree of thermal and spatial resolution. From these analyses, the instantaneous surface temperature distribution and transient surface temperature profile were obtained for a range of initial temperatures and impinging mass fluxes. The surface temperat was found to decay exponentially with time to a steady state value for the fluxes used. Thre dimensional plots of the temperature distribution on the surface also showed the significant lowering of the average surface temperature, and provided a qualitative description of the cooling phenomena at various stages during the transient. Results obtained will be used in t future validation of a computer model of the phenomena.

KEY WORDS (MAXIMUM 9 KEY WORDS; 28 CHARACTERS AND SPACES EACH; ALPHABETICAL ORDER; CAPITALIZE ONLY PROPER NAMES)

cooling; drop sizes; droplets; evaporation; solid surfaces; water

AVAILABILITY

[X] UNLIMITED [ ] FOR OFFICIAL DISTRIBUTION. DO NOT RELEASE TO NTIS.
[ ] ORDER FROM SUPERINTENDENT OF DOCUMENTS, U.S. GPO, WASHINGTON, D.C. 20402
[X] ORDER FROM NTIS, SPRINGFIELD, VA 22161

NOTE TO AUTHOR(S) IF YOU DO NOT WISH THIS MANUSCRIPT ANNOUNCED BEFORE PUBLICATION, PLEASE CHECK HERE. [ ]

ELECTRONIC FORM